JACS
JOURNAL OF THE AMERICAN CHEMICAL SOCIETY
pubs.acs.org/JACS
Article

The Milstein Bipyridyl PNN Pincer Complex of Ruthenium Becomes a Noyori-Type Catalyst under Reducing Conditions

Louise N. Dawe, Morteza Karimzadeh-Younjali, Zengjin Dai, Eugene Khaskin,* and Dmitry G. Gusev*

Cite This: https://dx.doi.org/10.1021/jacs.0c06518
Read Online

ABSTRACT: Hydrogenation of the dearomatized PNN ligand of the Milstein bipyridyl complex RuH(CO)[PNN] (**2**) gives a square-pyramidal Ru(II) product RuH(CO)[pPNN] (**5**). The central ring of the pPNN ligand is a piperidine. A minor byproduct of the hydrogenation reaction is complex **6** which has a dimeric structure made of two Ru(II) fragments each possessing a partly hydrogenated PNN ligand. The structures of **5** and **6** have been elucidated by NMR spectroscopy and X-ray crystallography. The PNN ligand of **2** is also hydrogenated under the conditions of the catalytic dehydrogenative coupling of ethanol to ethyl acetate. No direct evidence of the aromatized dihydride $RuH_2(CO)[PNN]$ (**4**) was found in this study. However, treating RuHCl(CO)[PNN] with $Li[HBEt_3]$ or reacting **2** with H_2 at low temperature resulted in a structurally characterized hydride-bridged dimer (**7**) bearing intact aromatized bipyridyl ligands. M06-L/def2-QZVP DFT calculations provided insights into the thermodynamics of the stoichiometric reactions of this work and into the nature of the intermediates of the catalytic ester hydrogenation facilitated by $RuH_2(CO)[pPN(H)N]$ (**8**) formed from **5** under H_2.

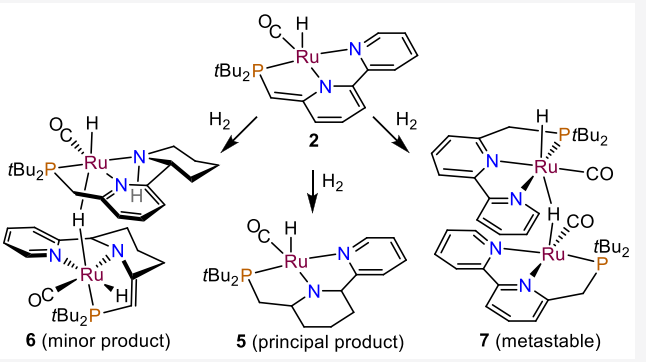

INTRODUCTION

The discovery of the ruthenium complexes **1** and **2** (Scheme 1)[1−5] and the concurrent paradigm development of metal–ligand cooperation in substrate activation by ligand aromatization–dearomatization have attracted much attention and discussion in the recent literature.[6−24] An important reaction of the 16-electron **1** is H_2 addition to give the well-characterized 18-electron dihydride **3** of Scheme 1.[1,5,25] Surprisingly, no experimental study of **2** has documented the analogous bipyridyl-based PNN dihydride **4**,[26−43] although this complex featured prominently in the proposed mechanisms of the catalytic reactions of **2**.[44−49]

Herewith, we present a study demonstrating that **4** is an unstable species of which no direct evidence could be obtained because of a facile H_2 loss resulting in formation of a hydride-bridged dimer. Under reducing conditions, either under H_2 in a hydrocarbon solvent or upon heating in ethanol, the pyridine fragments of the PNN ligand of **2** are hydrogenated. The product compounds are highly active Noyori-type catalysts for ester hydrogenation. A detailed mechanism of the catalytic ester reduction with one of these catalysts is presented, supported by experiment and DFT calculations.

Scheme 1. Milstein PNN Complexes of Ruthenium

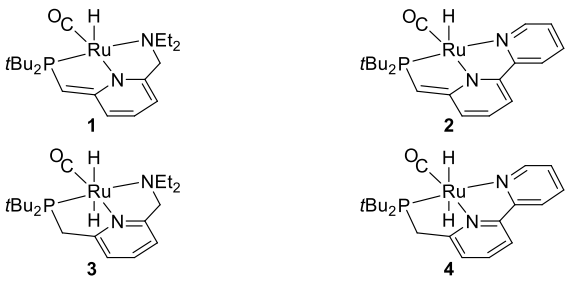

EXPERIMENTAL OBSERVATIONS

This study started with an attempt to obtain **4** following the procedure reported for **3**.[25] Thus, a solution of **2** in a mixture of benzene and hexane (1:1.8 v/v) was pressurized under 50 bar H_2 for 4 h. The color changed from the dark green of **2** to dark red-brown; however no product crystallized. This solution was repressured with H_2 and left standing for 3 days. Independently, **2** was reacted with H_2 (50 bar) for 2 h at 100 °C in hexane and in benzene. ^{31}P NMR spectra of the product solutions are compiled in Figure 1, and they exhibit several common resonances

Received: June 16, 2020

https://dx.doi.org/10.1021/jacs.0c06518
J. Am. Chem. Soc. XXXX, XXX, XXX−XXX

assigned to new complexes **5** and **6**. The details of product isolation and characterization are given below.

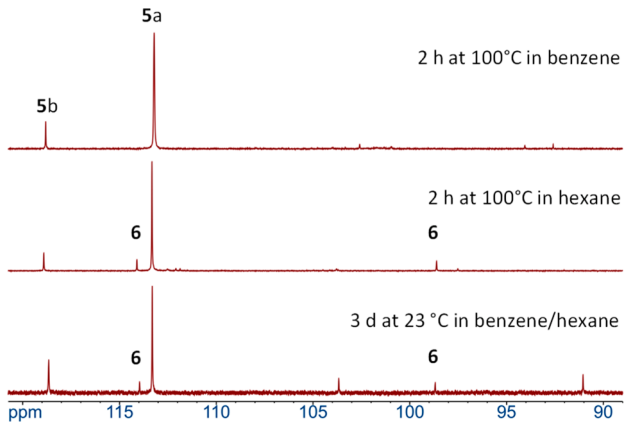

Figure 1. $^{31}P\{^{1}H\}$ NMR spectra of solutions produced by reacting **2** under 50 bar H_2.

Complex **5** was isolated from the benzene reaction solution of Figure 1. Evaporation of the solvent, followed by crystallization from hexane at −25 °C, afforded an extremely air-sensitive yellow solid (0.18 g, 70% yield). The product is well-soluble in hexane at room temperature, and it is highly soluble in C_6D_6 where it exists as a 9:1 mixture of isomers (^{31}P NMR, δ 113 (main isomer), 118 (minor isomer)). Slow recrystallization of **5** from hexane at −25 °C produced a sample for X-ray analysis that established the distorted square-pyramidal molecular geometry presented in Figure 2 and assigned to **5a** on the basis of the

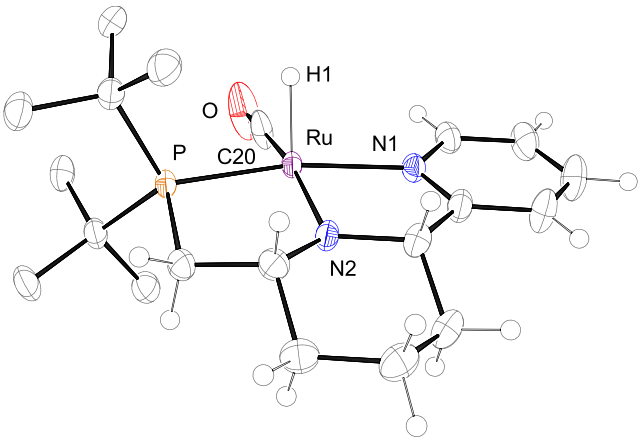

Figure 2. Structure of **5a** with the thermal ellipsoids at 50%. Hydrogens of the *tert*-butyl groups have been removed for clarity. Selected bond distances (Å) and angles (deg) are the following: Ru−P 2.2706(7), Ru−N1 2.1103(18), Ru−N2 1.9740(19), Ru−C20 1.835(3), Ru−H1 1.51(6), N1−Ru−P 162.99(5), N2−Ru−P 83.93(5), N2−Ru−N1 79.07(7), C20−Ru−P 96.75(7), C20−Ru−N1 99.78(9), C20−Ru−N2 164.57(10), H1−Ru−N2 113(3).

NMR data (vide infra). This structure is reminiscent of **2**; however, the central ring of the PNN ligand of **5a** is a piperidine. Overall, **5a** is a formally 16-electron Ru(II) complex where the amido N2−Ru bond is short, 1.974(2) Å, indicating a double-bond character (a single N(sp^3)−Ru bond length is 2.19 Å on average, when trans to CO, according to the Cambridge Structural Database). The hydrogenated pincer ligand of **5a** will be further referred to as pPNN; thus the complex is formulated as RuH(CO)[pPNN].

NMR data for the main isomer **5a** are consistent with the structure of Figure 2. The hydride resonance is observed at −18.48 ppm, whereas the CH protons of the piperidine fragment resonate at 3.90 and 3.30 ppm. NOE (nuclear Overhauser effect) measurements demonstrated a NOE between the CH protons; their NOEs to the hydride were also observed, in agreement with their spatial proximity seen in Figure 2. These experiments further established that the CH at 3.30 ppm is proximal to the PCH_2 protons, whereas the CH at 3.90 ppm is close to the pyridine ring. Complex **5** possesses three chiral centers (if the piperidine ring is conformationally nonrigid), and it can exist as a mixture of diastereomers. For example, isomer **5b** may differ from **5a** by the orientation of the Ru−H bond with respect to the pPNN ligand plane.

A minor product of the reactions of Figure 1, complex **6**, conveniently crystallized directly from the reaction solutions. This facilitated the structure characterization by X-ray crystallography and NMR spectroscopy. The crystals obtained from the hexane and benzene/hexane solutions of Figure 1 were independently analyzed by X-ray diffraction. The complex structure proved to be the same in both samples. This structure is presented in Figure 3 and in Scheme 2.

The molecule of **6** is made of two Ru(II) units, each possessing a hydrogenated PNN ligand, however hydrogenated in different fragments: in the central ring in one and in the terminal Py group of the former PNN ligand in the other Ru(II)

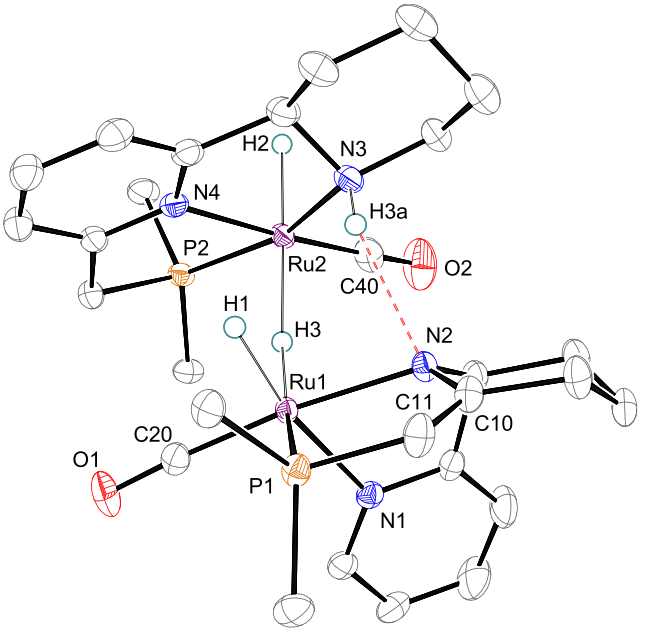

Figure 3. Structure of **6** with the thermal ellipsoids at 50%. The methyl groups and most hydrogen atoms are not shown for clarity. Selected bond distances (Å) and angles (deg) are the following: Ru1−H1 1.568(17), Ru1−H3 1.76(3), Ru1−P1 2.2996(7), Ru1−N1 2.184(2), Ru1−N2 2.1352(19), Ru1−C20 1.817(2), Ru2−H3 1.81(3), Ru2−H2 1.566(17), Ru2−P2 2.2704(7), Ru2−N4 2.097(2), Ru2−N3 2.172(2), Ru2−C40 1.835(3), P1−C11 1.780(3), C10−C11 1.357(4), C10−N2 1.374(3), N1−Ru1−P1 106.85(5), N2−Ru1−P1 82.00(5), N2−Ru1−N1 75.59(7), C20−Ru1−P1 94.66(8), C20−Ru1−N1 100.82(9), C20−Ru1−N2 174.04(9), N4−Ru2−P2 82.28(6), N4−Ru2−N21 78.00(8), N3−Ru2−P2 160.13(6), C40−Ru2−P2 96.11(8), C40−Ru2−N4 175.64(10), C40−Ru2−N3 103.38(10).

https://dx.doi.org/10.1021/jacs.0c06518
J. Am. Chem. Soc. XXXX, XXX, XXX−XXX

Scheme 2. Formation of the Minor Product, Dimer 6, from Complex 2

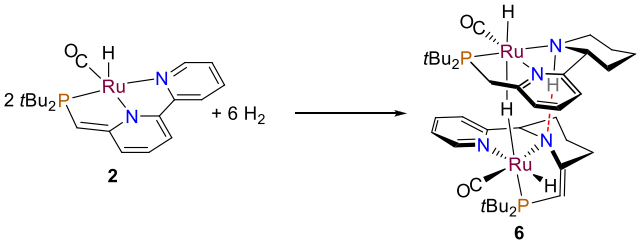

unit. Oddly, the C=C bond of dearomatized **2** survived the hydrogenation in one Ru unit, where the hydrogenated PNN ligand adopts an unexpected fac-coordination geometry (note the C10−C11 double bond distance of 1.357(4) Å). The two metal fragments are bridged by a single hydride (H3), and they are further connected by a weak N3−H3a···N2 hydrogen bond (H3a···N2 distance is long, 2.3 Å). The overall structure can be viewed as a product of addition of a 16-electron 5-coordinate amido Ru(II) monohydride (Ru1 fragment) onto an 18-electron octahedral Ru(II) dihydride (Ru2 fragment). The ^{1}H NMR spectrum of **6** is complicated; however the three hydride resonances are distinct at −10.47 (ddd, J = 23.4, 19.0, 5.0 Hz), −12.20 (ddt, J = 38.7, 5.9, 5.2 Hz), and −15.72 (dd, J = 30.1, 5.1 Hz) ppm. The ^{31}P NMR spectrum of **6** displays 1:1 peaks at 114 and 99 ppm. The unidentified minor species in the bottom spectrum of Figure 1 might be an isomer of **6**.

Additional experiments were attempted to produce dihydride **4** in solution. In one, RuHCl(CO)[PNN][3] was treated with ∼1.5 equiv of Li[HBEt$_3$] in THF-d_8. In two others, **2** was reacted with 1 atm H_2 in methylcyclohexane-d_{14} and in ethyl acetate, in J. Young NMR tubes. The NMR measurements were performed immediately after the sample preparation; particularly, the ethyl acetate solution was kept at −50 to −30 °C except when the tube was vigorously shaken in order to saturate the solvent with H_2. All three experiments cleanly produced deep turquoise solutions of the same product, complex **7**. The NMR spectra were best resolved between −50 and −30 °C; they became very broad at room temperature. Two 1:1 singlets were observed by ^{31}P{^{1}H} NMR at 105 and 123 ppm in THF-d_8. Two hydrides of **7** were apparent at −13.40 (ddd, J = 2.4, 16.0, 23.7 Hz) and −20.05 ppm (ddd, J = 4.3, 12.1, 16.0 Hz, in THF-d_8) exhibiting a mutual coupling, ^{2}J(HH) = 16.0 Hz. Fourteen protons were seen between 5.8 and 7.8 ppm, and four proton resonances of **7** appeared between 2.3 and 3.1 ppm. The NMR data are consistent with the formulation of **7** as a hydride-bridged dimer; the reactions leading to **7** are summarized in Scheme 3.

Complex **7** crystallized from the ethyl acetate solution upon standing overnight at room temperature, and the product structure of Scheme 3 was confirmed by X-ray crystallography (Figure 4). Dimer **7** can be viewed as an adduct of **4** with the four-coordinate 16-electron d^8-Ru$^{(0)}$(CO)[PNN]. The two metal fragments appear to be held together by a bridging hydride. The Ru−H1 distances are similar in Figure 4; however when optimized by DFT (vide infra), the structure develops a short Ru2−H1 (1.67 Å) bond and a long Ru1−H1 (2.14 Å) distance. This computational result agrees with the observation of unequal couplings: ^{2}J(H1−P2) = 12.1 Hz and ^{2}J(H1−P1) = 4.3 Hz. The crystallographic Ru1−Ru2 distance in **7** is 3.39 Å, and it is considerably shorter than the sum of the van der Waals radii, 4.1 Å, thus suggesting some metal−metal bonding. Metal oxidation states are ambiguous in this structure; e.g., one can view **7** as composed of two Ru$^{(I)}$H(CO)[PNN] fragments. A possibly very weak agostic interaction of Ru2 with the C38−H38c bond is present in **7**; however the Ru2−H38c distance is long, 2.67 Å.

Scheme 3. Formation of Dimer 7

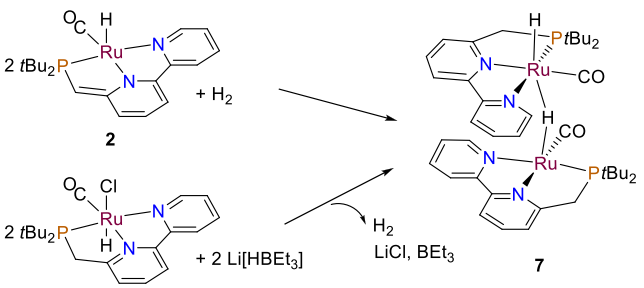

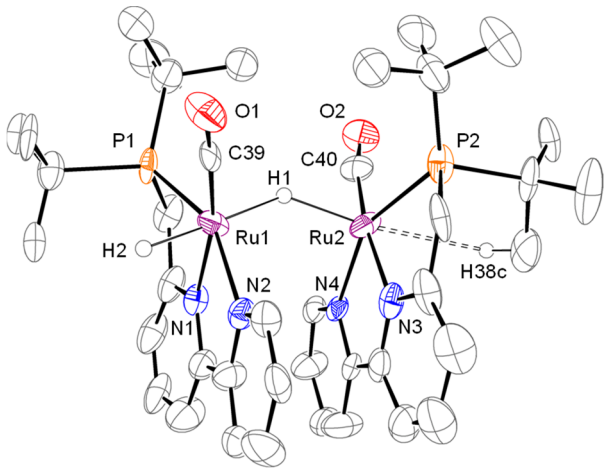

Figure 4. Structure of **7** with the thermal ellipsoids at 50%. Most hydrogen atoms are not shown for clarity. Selected bond distances (Å) and angles (deg) are the following: Ru1−H1 1.82(3), Ru1−H2 1.54(3), Ru1−P1 2.275(4), Ru1−N1 2.077(11), Ru1−N2 2.058(11), Ru1−C39 1.829(13), Ru2−H1 1.81(3), Ru2−P2 2.266(4), Ru2−N3 2.061(11), Ru2−N4 2.100(10), Ru2−C40 1.843(13), Ru2−H38c 2.67, N1−Ru1−P1 82.0(3), N2−Ru1−P1 153.0(4), N2−Ru1−N1 76.3(4), C39−Ru1−P1 95.8(4), C39−Ru1−N1 167.7(5), C39−Ru1−N2 102.0(5), N3−Ru2−P2 81.7(4), N3−Ru2−N4 78.4(4), N4−Ru2−P2 152.2(3), C40−Ru2−P2 98.0(5), C40−Ru2−N3 168.4(5), C40−Ru2−N4 97.6(5).

Complex **7** is not stable under H_2 in hydrocarbon solvents, and significant changes occur already in 2 h at room temperature in C_6D_6, illustrated in Figure 5 (bottom trace). The hydride resonances of **7** are seen there as the very broad lines near −13 and −20 ppm. Both isolated products, the major (**5**) and the minor (**6**), are apparently present in solution, and it seems that they are formed independently. Four sharp doublets seen between −19 and −25 ppm can be tentatively assigned to the intermediates (possibly diastereomers) formed by addition of one or two H_2 molecules to the PNN ligand of **2**.

Through the rest of this section, we report on some reactivity of complexes **2** and **5**. It might be already apparent from the spectra of Figure 1 that **5** *does not* form an isolable dihydride RuH$_2$(CO)[pPN(H)N] (**8**) as in Scheme 4. To probe whether dihydride **8** could be observable in solution, we prepared a sample of **5** in C_6D_6, under 1 atm H_2. The recorded ^{1}H NMR spectrum was virtually indistinguishable from that of **5** under Ar.

https://dx.doi.org/10.1021/jacs.0c06518
J. Am. Chem. Soc. XXXX, XXX, XXX−XXX

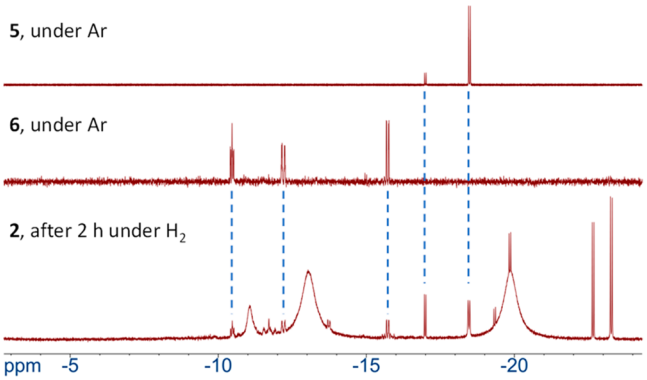

Figure 5. Hydride region of the ^{1}H NMR spectra of C_6D_6 solutions of **5** and **6** under Ar and **2** under 1 atm H_2 at 23 °C.

Scheme 4. Formation of Dihydride 8

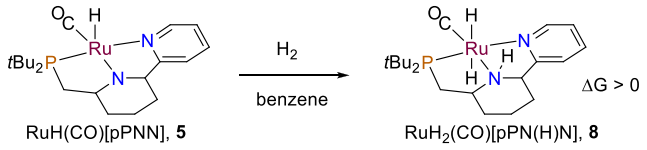

RuH(CO)[pPNN], **5** RuH$_2$(CO)[pPN(H)N], **8**

A signal of the dissolved H_2 was observed, indicating that formation of **8** is thermodynamically unfavorable.

Complex **5** reacts with ethanol at room temperature to give two species. In neat ethanol-d_6, these are in a approximately 10:1 ratio in the ^{31}P NMR spectrum at 98.5 and 100 ppm, respectively. The NMR spectra of the product, presumed to be the ethoxide RuH(OEt)(CO)[pPN(H)N] (**9**), are well-defined, although the hydride site is 95% deuterated in ethanol-d_6; the residual RuH is observable at −16.68 ppm (d, J(HP) = 26 Hz). A slow H/D exchange also occurs in **9** in one piperidine CH group, at 3.98 ppm. The d_5-ethoxide ligand of **9** was not observed in the ^{13}C NMR spectrum, presumably because of a rapid exchange with the solvent.

To compare the complexes of this work in catalytic hydrogenation, we tested them in the reduction of ethyl acetate (EA) and methyl hexanoate (MH). The results are compiled in Table 1. Under the solventless base-free conditions, complexes **5** and **6** proved to be highly efficient for the reduction of the esters to give the corresponding alcohols: ethanol, hexanol, and methanol. This is not too surprising in the case of **5** since the complex is closely related to several existing PNN hydrogenation catalysts of ruthenium and osmium.[50−55] Complex **5** is active for the reduction of ethyl acetate even at room temperature, affording TON = 630 in 3 h. The Milstein catalyst **3** was markedly less efficient under the reaction conditions of Table 1, although these may not be optimal with **3**. For instance, the catalytic efficiency of **3** toward EA was shown to be significantly better under basic conditions.[25]

Table 1. Catalytic Reduction of Ethyl Acetate (EA) and Methyl Hexanoate (MH)[a]

line	cat.[b]	ester[c]	% conv[d]	TON[e]
1	**2**	EA	18.0	1960
2	**2**	MH	23.5	2500
3	**3**	EA	2.4	240
4	**3**	MH	6.5	648
5	**5**	EA	89.5	8625
6	**5**	EA	31.5	630[f]
7	**5**	MH	61.2	6123
8	**6**	EA	97.8	9776
9	**6**	MH	91.7	8964

[a]3 h at 100 °C, initial $p(H_2)$ = 50 bar, in a 300 mL Parr reactor magnetically stirred at 500 rpm. [b]Catalyst, 2 × 10^{-5} mol. [c]Substrate, 0.2 mol. [d]Percent conversion of ester to alcohol. [e]Ester to alcohol turnover number. [f]At 25 °C, S/C = 2000.

The dearomatized **2** exhibited good catalytic activity toward the reduction of EA and MH, yet distinctly lower than that of **5** or **6**. The reduction of the PNN ligand of **2**, which was facile in the hydrocarbon solvents, might be somewhat retarded in an ester media. This idea is partly supported by the observation that complex **7** (formed from **2** under H_2) was relatively stable in and crystallized from ethyl acetate, under H_2. When a solution of 20 mg of **7** in ethyl acetate, sealed in a J. Young NMR tube under 1 atm H_2 (H_2/Ru molar ratio of ∼2.5), was heated at 80 °C for 2 h, the dimer persisted in solution and accounted for 64% of the total ^{31}P integral signal intensity. An estimated 2−3 equiv of ethanol was produced during this time, indicating that practically all hydrogen was consumed and that transfer of hydrogen from **7** to ethyl acetate was slow even at 80 °C. Formation of a new ruthenium hydride complex was observed in this solution (d, δ − 17.07, ^2J(H−P) = 26.3 Hz, (see Figure S30 for details).

Recently, Chianese published a reaction of **1** with PCy_3 in toluene at 100 °C that gave a Ru(0) imine product.[56] Under H_2, the imine was converted into a Noyori-type catalyst that proved to be competent for ester hydrogenation. We briefly checked whether the Milstein catalyst complex **3** is stable at 100 °C under 50 bar H_2. Two experiments in benzene, with heating for 2 and 4 h, respectively, gave similar results. Two peaks dominated the ^{31}P NMR spectra of the product solutions, at 124 and 117 ppm, contributing approximately 20% and 55% to the total ^{31}P signal integration, respectively, after 4 h of heating. The former chemical shift corresponds to **3**, whose hydrides were observed at −4.18 ppm. The latter is an unknown species, associated with three hydride resonances at −7.54 (t, J(HP) = 7.2 Hz), −9.61 (t, J(HP) = 54.5 Hz), and −10.65 (non-first-order m), in a 1:1:2 ratio. Further studies of the product (evaporated and redissolved in C_6D_6) identified the resonances of the pyridine protons (δ 8.01 (d), 7.16 (t), and 6.71 (d)) and those of the diastereotopic protons of the CH_2 groups (δ 5.05 (d), 4.68 (d), 3.49 (dd) and 3.13 (dd)), each of these integrated as 2H vs the hydrides. The NCH_2 resonance of the ethyl groups appeared at 2.79 ppm as a quartet of integration 8H. The NMR data indicate a dimeric structure possessing an intriguing symmetry but do not allow a reliable structural assignment. Nevertheless, these experiments confirmed that **3** persists upon heating under H_2 at 100 °C, and the two principal species in solution possess an intact 2-(CH_2P*t*Bu_2)-6-(CH_2NEt_2)-C_6H_3N ligand on ruthenium.

In the final experiment, we pursued the question of whether the PNN ligand of complex **2** might undergo hydrogenation under the conditions of the catalytic acceptorless alcohol dehydrogenation. This was probed by heating a solution of **2** in ethanol (0.067 M) at 80 °C in a J. Young NMR tube vented through the top via a piece of tubing connected with a bubbler. NMR spectra were recorded after 2 and 6 h of heating; these spectra exhibited only minor differences. The principal product was observed at 100 ppm in the ^{31}P{^{1}H} NMR; the integration of this peak changed from 81% (2 h) to 88% of the total ^{31}P NMR signal after 6 h of heating. The hydride resonance of the product appeared at −17.54 ppm (d, J = 26.4 Hz). Formation of

https://dx.doi.org/10.1021/jacs.0c06518
J. Am. Chem. Soc. XXXX, XXX, XXX−XXX

ethyl acetate was evident from the spectra; the TON (turnover number) of ethanol to ethyl acetate of 26 and 34 was recorded in 2 and 6 h, respectively. The ^{1}H and ^{13}C{^{1}H} NMR shifts of the pincer ligand of the main product closely match those of the ethoxide **9**. Thus, the NMR observations unambiguously confirm that the PNN ligand of **2** is hydrogenated under the conditions of the dehydrogenative coupling of ethanol. When analyzing the ^{13}C NMR spectrum (Figure S16), we noticed two peaks at 181.9 and 25.4 ppm, the shifts being similar to those of the acetate ligand of RuH(OAc)(CO)[HN(CH$_2$CH$_2$P*i*Pr$_2$)$_2$] (181.4 and 26.1 ppm) reported by Gauvin and co-workers.[57] The acetate could form as a result of the dehydrogenative coupling of ethanol with a trace amount of water in the solvent; this chemistry is well-documented.[57] It is reasonable to postulate that **9** might form during the reaction of **2** with ethanol, according to Scheme 5; however the more stable acetate complex **10** is the thermodynamic product in ethanol containing adventitious water.

Scheme 5. Reduction of 2 in Ethanol

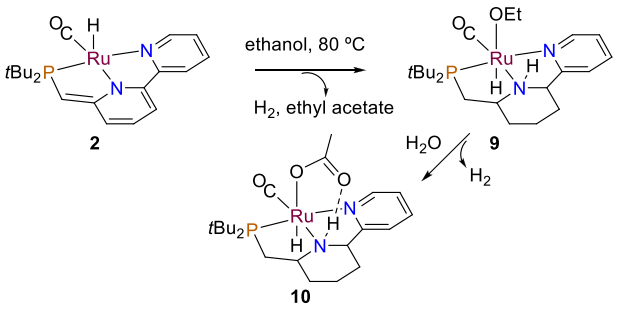

DFT COMPUTATIONAL DATA

Reactions of the complexes of this work were investigated with the help of M06-L/def2-QZVP DFT calculations. We shall first look at the stoichiometric transformations of **2**, **4**, and dimer **7** in benzene, summarized in Scheme 6. Isomerization of **2**, leading to the square-planar Ru$^{(0)}$(CO)[PNN] species is unfavorable, yet the product singlet structure is only marginally less stable. Considering the reaction barrier of 36.8 kcal/mol from **2**, the isomerization is expected to be slow at room temperature.

Formation of **4** from **2** under 1 atm H_2 is a favorable process. Therefore, the reason why **4** has not been observed must be due to relatively fast dimerization leading to **7**. Indeed, the formation of the dimer is exergonic by −12.3 kcal/mol. Considering the dissociation reactions of **7** of Scheme 6, it is clear that the release of **4** back (together with Ru(CO)[PNN]) is unlikely, being 18.3 kcal/mol uphill. It is however possible that **7** can split to give a trace of the paramagnetic 17-electron species Ru$^{(I)}$H(CO)-[PNN].

Formation of the isolated products **5a** and **6** in Scheme 7 is accompanied by the relatively large Gibbs energies of −14.0 and −16.3 kcal, respectively, per mole of **2** reacted. Finally, formation of dihydride **8** is indeed thermodynamically unfavorable, in agreement with the experimental observations.

In Scheme 8, we are looking at the energies of ethanol addition to **5a** and hydrogen bonding of ethanol with **8** and **9**. Formation of ethoxide **9** is an endergonic process; however the product is stabilized by hydrogen bonding with ethanol in **9**·EtOH. We should treat **9**·EtOH as a minimal model of this species. Similarly, **8** can favorably bind a molecule of EtOH.

Scheme 6. Calculated Reaction Gibbs Energies of the Stoichiometric Transformations of 2, 4, and Dimer 7[a]

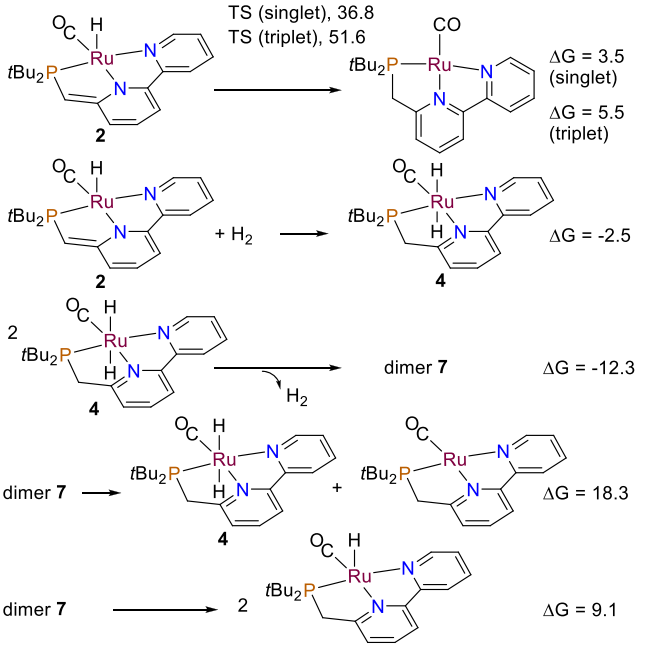

[a]Calculated in benzene solvent continuum (all 1 M solutes, at 298.15 K, $p(H_2)$ = 1 atm). The energies of the reactions of **7** are per mole of the dimer formed or reacted.

Scheme 7. Calculated Reaction Gibbs Energies for 2 and 5a with H_2[a]

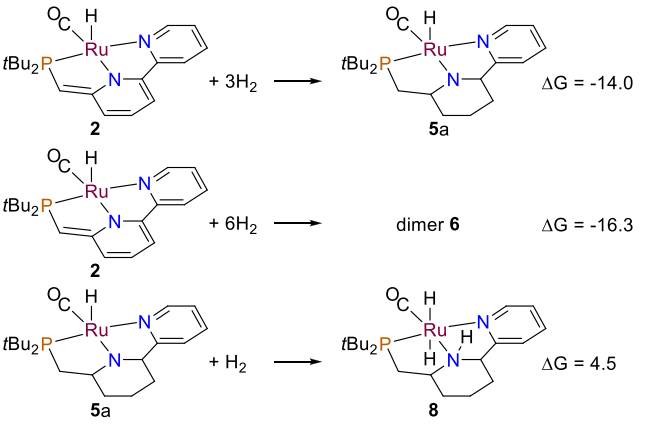

[a]Calculated in benzene solvent continuum (all 1 M solutes, at 298.15 K, $p(H_2)$ = 1 atm). Mass balance is ensured throughout.

Next, a plausible mechanism of the catalytic reduction of ethyl acetate to ethanol with **5a** under $p(H_2)$ = 50 atm was calculated, following the ideas of others and those of our own.[22,25,53,57−65] The results are organized in the form of the catalytic cycle of Scheme 9. Two sets of energies are given there. The first is vs **5a**; e.g., the entry into the catalytic cycle, **8**·EtOH, is at 0.4 kcal/mol. The second set of energies (given in parentheses) is vs **9**·EtOH, and then **8**·EtOH is at 1.1 kcal/mol. The systematic difference between the two energy sets is negligible, 0.7 kcal/mol. Nevertheless, it is important to recognize that once the catalytic reaction has generated enough alcohol, the most stable ruthenium species in solution is **9**·EtOH. All structures of

https://dx.doi.org/10.1021/jacs.0c06518
J. Am. Chem. Soc. XXXX, XXX, XXX−XXX

Scheme 8. Calculated Reaction Gibbs Energies for 5a and 8 with EtOH[a]

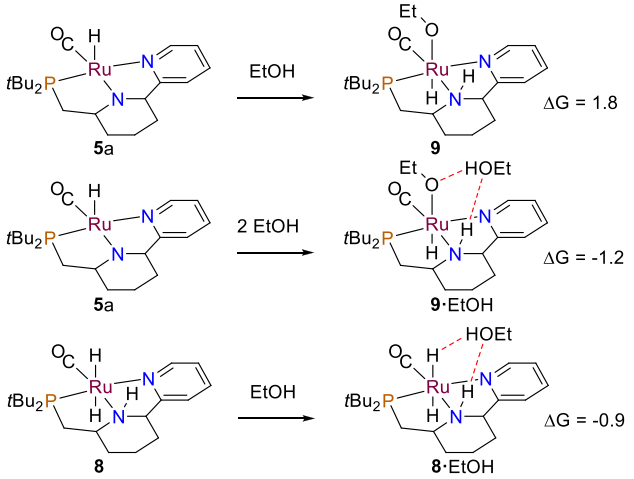

[a]Calculated in benzene solvent continuum (all 1 M solutes, at 298.15 K).

Scheme 9. Catalytic Hydrogenation of Ethyl Acetate with 8[a]

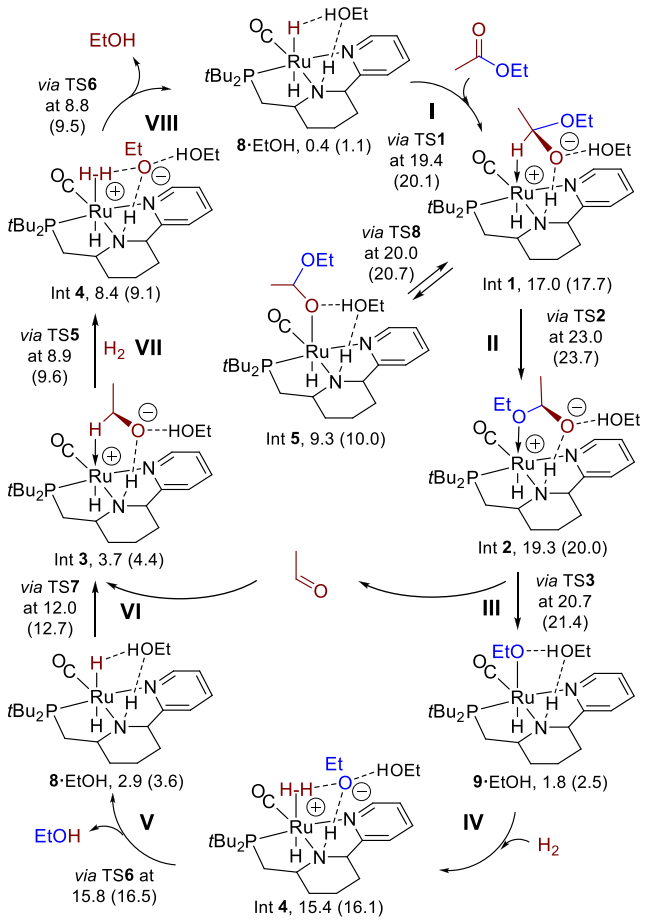

[a]M06-L/def2-QZVP Gibbs energies (kcal/mol) of the species in ethyl acetate solvent continuum (all 1 M solutes, at 298.15 K, under 50 atm H_2) vs **5a** + EtOH + H_2, or (in parentheses) vs **9**·EtOH + H_2. Mass balance is ensured throughout.

Scheme 9 were optimized in ethyl acetate solvent continuum; thus, the ester is both the solvent and the substrate.

The hydrogenation starts by a hydride transfer to ethyl acetate in step I. With TS**1** at 19.4 (20.1) kcal/mol, this should be facile. The product zwitterionic 1-ethoxyethoxide complex Int **1** may rearrange to give Int **5**; however the productive pathway from Int **1** is step II, to Int **2**. It is this step that encounters the largest barrier in the catalytic cycle, TS**2** at 23.0 (23.7) kcal/mol. The height of this barrier agrees with the observation that the reduction of ethyl acetate with **5** was relatively fast at 25 °C (Table 1, line 6). Elimination of acetaldehyde from Int **2** in step III is practically barrierless; this gives the ethoxide **9**·EtOH.

Step IV of Scheme 9 proved challenging to calculate. Two plausible scenarios of the ethoxide substitution by H_2 were investigated: unimolecular S_1 and bimolecular S_2. The S_1 process starts by elimination of the ethoxide to give a 16-electron cationic ruthenium intermediate that subsequently adds H_2. S_2 is a bimolecular reaction where the ethoxide is displaced by H_2. Attempts to find the corresponding transition states have been unsuccessful. What became apparent when working on the S_1 process was the tendency of the ethoxide, upon elimination, to rearrange into an agostic species Int **3** via TS**4**, as shown in Scheme 10. Then, the agostic ethoxide can be displaced by H_2 via TS**5**, affording the dihydrogen complex Int **4**.

Scheme 10. Composite Step IV

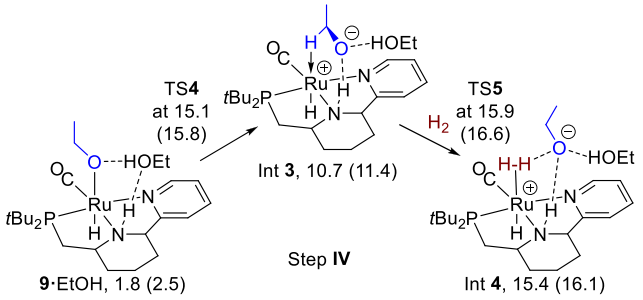

The rest of the catalytic cycle is straightforward. Deprotonation of the H_2 ligand of Int **4** in step V of Scheme 9 is facile. This regenerates the catalyst **8**·EtOH, followed by insertion of the aldehyde intermediate in step VI. The product, agostic ethoxide Int **3**, undergoes substitution with H_2 in step VII. The catalyst **8**·EtOH is regenerated once again after deprotonation of the dihydrogen ligand of Int **4** in step VIII. The overall process, EtOAc + 2H_2 (50 atm) → 2EtOH, is accompanied by ΔG = −4.5 kcal/mol. A perhaps more accurate energy of this organic reaction is ΔG = −7.2 kcal/mol, calculated using the M06-2X/def2-QZVP method which is better suited for main-group thermochemistry than M06-L/def2-QZVP that we prefer for organometallic reactions of transition metal complexes.[66,67]

The events of Scheme 9 do not involve the conventional metal−ligand cooperation (MLC) often associated with the Noyori-type catalysts.[22] MLC ideas envisage that "the non-innocent ligands *directly* participate in the substrate activation and *in the bond formation*" in the metal−ligand cooperating bifunctional catalysts.[68] Thus, a mechanism was considered here where the transfer of a metal hydride *and* the NH proton of **8**·EtOH to ethyl acetate gave 1-ethoxyethanol according to Scheme 11. The energy of this reaction, EtOAc + **8**·EtOH → 1-ethoxyethanol + **5a** + EtOH, is the energy of hydrogenation of ethyl acetate: EtOAc + H_2 (50 bar) → 1-ethoxyethanol, when **8**·EtOH is referenced to **5a** + EtOH + H_2 (50 atm) as in Scheme 9. This organic reaction energy was calculated to be 9.8 and 4.0 kcal/mol with the M06-L/def2-QZVP and M06-2X/def2-

https://dx.doi.org/10.1021/jacs.0c06518
J. Am. Chem. Soc. XXXX, XXX, XXX−XXX

Scheme 11. Formation and Splitting of 1-Ethoxyethanol[a]

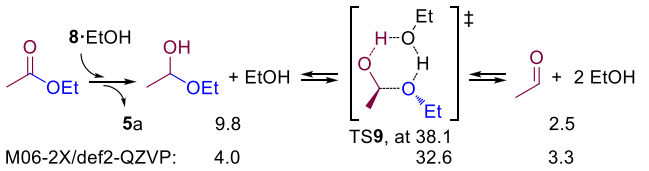

[a]The reaction Gibbs energies (kcal/mol) are in ethyl acetate solvent continuum (all 1 M solutes, at 298.15 K). Mass balance is ensured throughout.

QZVP methods, respectively, the latter value being presumably more accurate.

1-Ethoxyethanol can split into acetaldehyde and ethanol in solution. A slow equilibrium between these species was indeed observed by solution NMR spectroscopy, and the reaction energy of 0.3 kcal/mol was estimated from the equilibrium constant in ethanol, at room temperature.[51] The M06-2X/def2-QZVP value of $\Delta G = 3.3 - 4.0 = -0.7$ kcal/mol calculated in ethyl acetate is reasonably consistent with the experiment. As is apparent from Scheme 11, transition state TS**9** for the ethanol-assisted C−O bond cleavage of 1-ethoxyethanol is at 32.6 kcal/mol (M06-2X/def2-QZVP energy), and this process is unfavorable considering the much lower barrier TS**2**, 23.0 kcal/mol, in step II of Scheme 10. While the formation of 1-ethoxyethanol is not precluded, this and the organic reaction of Scheme 11 via TS**9** seem catalytically irrelevant.

We also calculated barrier TS**10** for H_2 addition to complex **5a**. TS**10** is at 21.5 kcal/mol vs **5a** and H_2 (50 atm). When **5a** originates from **8**·EtOH and ethyl acetate according to Scheme 12, then **5a** is at 2.5 kcal/mol and TS**10** is at 24.1 kcal/mol. This

Scheme 12. H_2 Addition to Complex 5a[a]

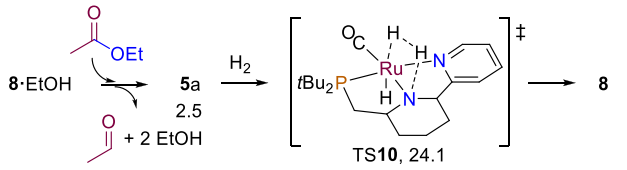

[a]M06-L/def2-QZVP Gibbs energies (kcal/mol) of the species in ethyl acetate solvent continuum (all 1 M solutes, at 298.15 K, under 50 atm H_2) vs **5a** + EtOH + H_2. Mass balance is ensured throughout.

barrier is too high (vs TS**5** at 15.9 kcal/mol) for the reaction to proceed via the conventional MLC mechanism. The ethoxide substitution by H_2, illustrated in Scheme 10, is a lower energy process for the regeneration of the dihydride catalyst. It is, of course, counterintuitive that H_2 addition to the five-coordinate complex **5a** should be a higher-energy process compared to the same reaction of the octahedral complex **9**·EtOH.

A further argument could be made that the H_2 splitting on **5a** might be facilitated by ethanol via Int **7** and TS**11** of Scheme 13. The energy of TS**11** is indeed lower than that of TS**10**, 17.8 vs 24.1 kcal/mol. However, the ethanol competes with H_2 in the reaction with **5a**. Ethanol addition to **5a** gives Int **8**, then ethoxide **9** via TS**12**. When enough ethanol is present, complex **9**·EtOH will be formed, the overall reaction **5a** + 2EtOH → **9**·EtOH being an exergonic process, as was already noted in Scheme 8. The energy differences between the two competing pathways of Scheme 13 favor ethanol addition to **5a** when [EtOH] ≥ [H_2]. The mole fraction solubility of H_2 in ethyl

Scheme 13. H_2 vs EtOH Addition to 5a[a]

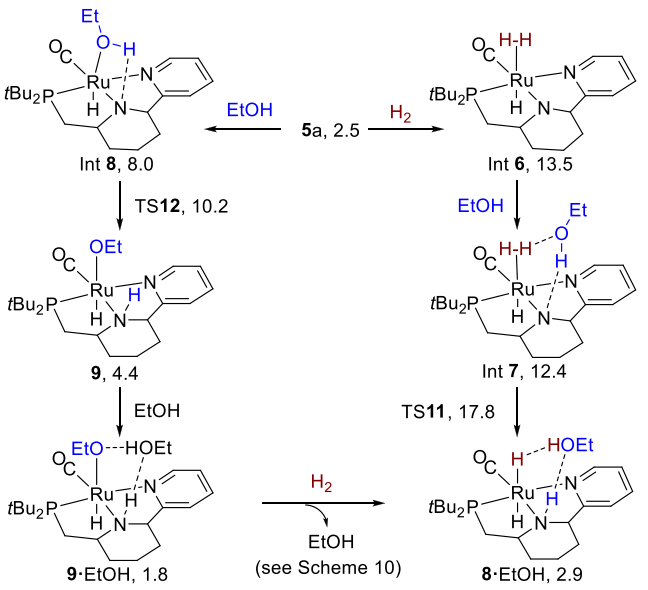

[a]M06-L/def2-QZVP Gibbs energies (kcal/mol) of the species in ethyl acetate solvent continuum (all 1 M solutes, at 298.15 K, under 50 atm H_2) vs EtOAc + **5a** + EtOH + H_2. Mass balance is ensured throughout.

acetate is ~3.5×10^{-4} under 1 atm H_2 at 298 K.[69] When EtOAc/**5a** ratio is 10^4 (the *S*/*C* ratio in Table 1), the corresponding H_2/**5a** ratio is ~3.5. This ratio will increase with increased $p(H_2)$ and temperature; nevertheless, when ethyl acetate conversion to ethanol would reach 1% (TON = 100, or 200 equiv of alcohol produced), the likelihood of formation of the dihydrogen complex Int **6** from **5a** (if the latter is present) should become negligible, and the proton shuttle pathway of Scheme 13 can be safely ignored as a mechanism of the dihydride catalyst regeneration. Through most of the catalytic reaction, the catalyst **8**·EtOH originates from **9**·EtOH via Int **3**, as illustrated in Schemes 9 and 10.

DISCUSSION

Complex **2** has been used in a large variety of catalytic reactions. Hydrogenations of amides, urea derivatives, carbamates, carbonates, esters, and nitriles with **2** have been reported, summarized in Scheme 14.[3−5,26,29,30,38,40] Rearomatization of the PNN ligand of **2** and formation of a dihydride intermediate under H_2 were suggested in the proposed mechanisms.[3,5,30] Dehydrogenative coupling reactions of alcohols have also been successful with **2**. The precursor to **2**, RuHCl(CO)[PNN] (**11**),[3] could also be used, in combination with a base. These catalytic reactions included cross-dehydrogenative coupling of primary alcohols with secondary alcohols or amines, coupling of diols and diamines, and coupling of amino alcohols with secondary alcohols, according to Scheme 15.[27,28,32−36,39] The dehydrogenative olefination of alcohols using a Wittig reagent was demonstrated.[41] Two miscellaneous catalytic reactions of **11** via **2** involved CO oxidation by N_2O and the selective deuteration of alcohols in D_2O.[31,43] Reactions of Scheme 15 were proposed to proceed via the initial formation of an aromatized alkoxide complex from **2** and the substrate alcohol.

Although a major effort has been put into the study of the catalytic activity of **2**, little is known about the stoichiometric reactivity of this complex. Addition of acetic or formic acid led to

https://dx.doi.org/10.1021/jacs.0c06518
J. Am. Chem. Soc. XXXX, XXX, XXX−XXX

Scheme 14. Hydrogenation Reactions with 2[3−5,26,29,30,38,40]

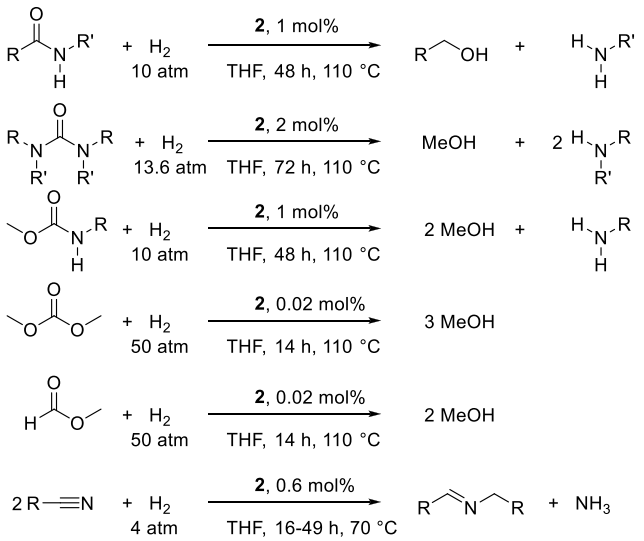

Scheme 15. Dehydrogenative Coupling with 2 and 11[27,28,32−36,39,41]

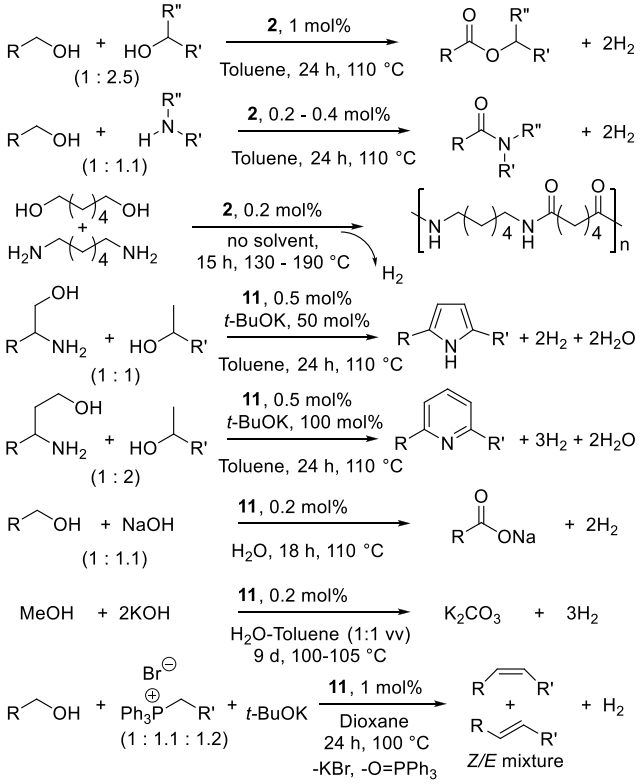

the expected octahedral aromatized Ru(II) carboxylate complexes.[35,36] Similarly, **2** with water gave the aromatized Ru(II) hydroxide.[36] Finally, addition of CO to **2** afforded the octahedral dearomatized dicarbonyl product.[43] No study of reactions of **2** with H_2 or alcohols has been disclosed.

Despite the scarcity of information about the reactivity of **2**, seven computational studies[22,44−49] have been published to date that pursued different aspects of the catalytic mechanisms with **2**. Cantillo[44] and Zhang[47] independently modeled the catalytic hydrogenation of amides of Scheme 14. Both studies concluded that the reaction occurred via MLC involving aromatization/dearomatization of the PNN ligand. Complexes **2** and **4** featured prominently in the catalytic cycles. Li and Hall[45] and Hasanayn with co-workers[48] investigated the catalytic oxidation of primary alcohols in aqueous NaOH, resulting in the corresponding carboxylates. Although the proposed mechanisms differed significantly, dihydride **4** was their common catalytic intermediate. Wang and co-workers[46] computed a mechanism of the pyrrole synthesis of Scheme 15. Once again, the ideas of MLC by aromatization−dearomatization were pursued. Alcohol dehydrogenation on **2** was proposed to follow the so-called BDFT (bifunctional double hydrogen transfer) mechanism to give **4**. Dub and Gordon[22] re-examined the computation work of Wang and co-workers to point out that their "proton shuttle" was a nonexistent process. Finally, Gonçalves and Huang performed a computational analysis of the aromaticity changes upon the heterolytic H_2 cleavage on **2** to give **4**.[49] No study mentioned above was evidence-based.

Our work does not imply that complex **2** itself is not a capable catalyst of ester hydrogenation and alcohol dehydrogenative coupling, without formation of a piperidine-type ligand. However, the sticking point of the calculated mechanisms is the assumption of sustained presence of catalytically relevant concentrations of **2** and **4** under H_2 or in alcohols over the 24−48 h reaction times of Schemes 14 and 15. The involvement of complexes **5**−**9** (and the intermediates leading to these complexes) in the catalytic reactions of Schemes 14 and 15 cannot be ignored. This situation serves as a warning that while DFT studies offer valuable insights, they can be biased, unduly narrow in scope, and inconclusive. This may happen when little is known about the underlying chemistry; however, the theoretical modeling can also be flawed. For example, a meaningful computational study of hydrogen ion (H^+/H^-) transfers and the resulting ionic reaction intermediates requires geometry optimizations in a solvent continuum, in conjunction with explicit solvation when hydrogen bonding is important. The relatively widespread gas-phase DFT modeling of MLC is inappropriate because the stationary points found in the gas phase may not exist in solution and vice versa.[22,60−64,70]

The meaning of "cooperation" or "cooperativity" in MLC is somewhat open to interpretation, as the terms are not specific. The conventional MLC mechanisms[22] with the Noyori-type systems seem to have one common feature: their catalytic cycles all include a formal 16-electron intermediate. Thus, "the *non-innocent* ligands directly participate in the substrate activation and *in the bond formation*."[68] These ideas have been rebuked in recent years.[22,60−64] The modern understanding of MLC is that the cooperating ligand is *innocent* in the catalytic hydrogenation and dehydrogenative coupling reactions with the Noyori-type catalysts. Our calculations are in full accord with this understanding. The five-coordinate amido complex **5a** is an off-cycle species in the mechanism of Scheme 9 where the catalyst is the dihydride complex **8**. Another important species in the cycle is alkoxide **9**·EtOH. We already extensively commented on this intermediate that should be thermodynamically and kinetically labile to allow facile regeneration of the dihydride catalyst under H_2.[25] All intermediates of Schemes 9 and 10 are octahedral Ru(II) complexes where the reacting organic moiety is hydrogen-bonded to the NH group of the pPN(H)N ligand which forms a reaction "pocket" where the substrate is optimally oriented, activated, or stabilized.

The hydrogenation of **2**, documented in this study, is not unprecedented. Similarly, the phenanthroline-based PNNP ligand of ruthenium complex **12** of Scheme 16 undergoes facile

https://dx.doi.org/10.1021/jacs.0c06518
J. Am. Chem. Soc. XXXX, XXX, XXX−XXX

Scheme 16. Examples of PNNP and PN Ligand Hydrogenation[71−74]

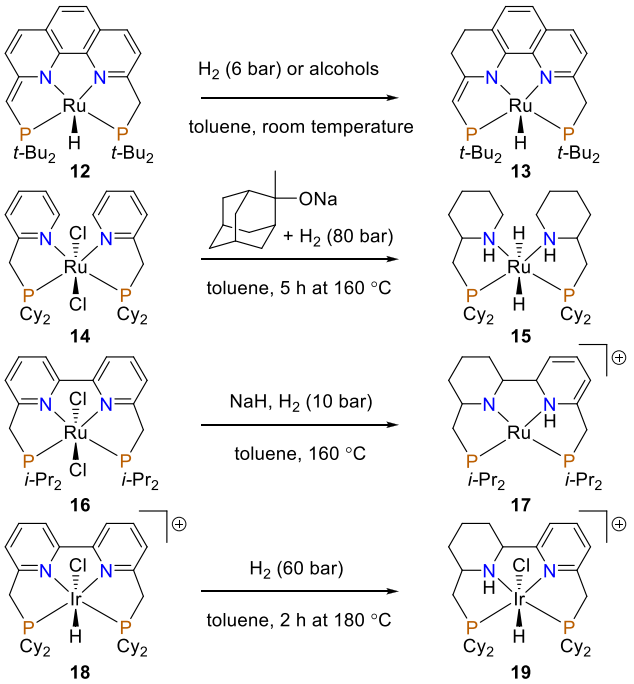

hydrogenation under H_2 or when reacted with methanol or hexanol.[71] The hydrogenation of **12** was not studied at 110 °C when this system becomes active for the dehydrogenative coupling of primary alcohols. Saito and co-workers observed hydrogenation of the pyridine and bipyridine fragments of ruthenium complexes **14** and **16** (Scheme 16) upon heating, under basic conditions, to give the Noyori-type catalysts **15** and **17**, respectively.[72,73] The bipyridine fragment of **16** underwent a full hydrogenation and a P−C bond cleavage when the H_2 pressure was increased to 40 bar.[73] The related iridium hydridochloride **18** was hydrogenated under base-free conditions, first to give **19** after 2 h, then a fully hydrogenated product after 4 h of heating.[74] Considering that the PNN ligand of **2** has been used to make manganese,[75−78] iron,[79−83] and cobalt[84−88] catalysts, it is appropriate to suggest that mechanistic studies of these complexes must inquire into the nature of the metal species formed under conditions approximating the catalytic, i.e., using the relevant reaction temperature, time, and (when present) H_2 pressure.

In conclusion, our work and the examples of Scheme 16 comprise substantive evidence indicating that the heteroaromatic fragments of the coordinated PN, PNN, and related polydentate ligands may be susceptible to hydrogenation under reducing conditions. A notable exception is complex **3** that is relatively stable at 100 °C under 50 bar H_2. Theoretical studies of reactions of the metal complexes structurally related to **2**, **12**−**14**, and **16**−**19** should consider the previous studies detailing facile changes to the ligand architecture and should be supported by sufficient relevant experimental data.

MATERIALS AND METHODS

Experimental Details. Complexes **2** and **3** were prepared following the reported procedures.[3,25] All chemicals and solvents were purchased from Sigma-Aldrich. Anhydrous-grade solvents, ethyl acetate, and methyl hexanoate were stored and used in an argon drybox. The anhydrous deuterated solvents were stored and used in the same drybox, with 3 Å molecular sieves. The room-temperature NMR spectra were collected on a Agilent DD2 400 MHz spectrometer, and the low-temperature studies were conducted on a Varian Unity Inova 300 MHz instrument. For quantitative integration, the proton NMR spectra were acquired using 15° pulses and a relaxation delay of 30 s.

Complex 5. In an argon glovebox, the glass liner of a 75 mL Parr reactor was loaded with a 9.5 mm × 13 mm SCIENCEWARE rare-earth magnet spinbar, 0.25 g (0.56 mmol) of **2**, and 4 mL of benzene. The reactor was closed, removed from the glovebox, pressurized to $p(H_2)$ = 50 bar, and placed in an oil bath preheated to 100 °C. After 2 h of stirring, the reactor was moved into a cold-water bath for 30 min, then vented and returned into the glovebox. The dark product solution and the spinbar were transferred into a 25 mL pear-shaped flask, and the solvent was evaporated under vacuum, followed by drying of the golden-yellow solid for 1 h. The product was redissolved in 12 mL of hexane, and the product solution was filtered through a medium-porosity fritted funnel into a 20 mL vial. This vial was left in the freezer (−25 °C) of the glovebox overnight. The product crystallized, and the mother liquor was removed from the vial with a pipet; the remaining yellow crystalline material was dried under vacuum for 2 h. Yield: 176 mg (70%) of complex **5** containing ∼8 mol % of residual hexane. Elemental analysis was not attempted on this material because of the residual solvent and extreme air-sensitivity. NMR data (main isomer **5a**): ^{1}H NMR (400 MHz; C_6D_6): δ 9.06 (m, 1H), 6.75 (td, J = 7.8, 1.6 Hz, 1H), 6.59 (d, J = 7.8 Hz, 1H), 6.20 (t, J = 6.5 Hz, 1H), 3.90 (d, J = 11.3 Hz, 1H), 3.30 (m, 1H), 2.25 (ddd, J = 14.6, 10.5, 5.4 Hz, 1H), 1.95 (dm, J = 12.3, 1H), 1.84 (m, 2H), 1.67 (ddd, J = 14.6, 8.6, 7.6 Hz, 1H), 1.52 (qt, J = 13.1, 3.7 Hz, 1H), 1.33 (d, J = 9.8 Hz, 9H), 1.30 (d, J = 9.9 Hz, 9H), 1.14 (m, 1H), 1.00 (m, 1H), −18.48 (dt, J = 22.2, 2.2 Hz, 1H). ^{13}C{^{1}H} NMR (100 MHz; C_6D_6): δ 209.5 (d, J = 11.5 Hz, CO), 171.7 (d, J = 1.2 Hz, C), 154.0 (s, CH), 134.3 (s, CH), 121.6 (d, J = 2.1 Hz, CH), 120.9 (d, J = 1.0 Hz, CH), 74.6 (d, J = 3.3 Hz, NCH), 67.4 (d, J = 6.3 Hz, NCH), 37.9 (d, J = 11.4 Hz, CH_2), 36.8 (d, J = 16.4 Hz, CH_2), 35.9 (d, J = 18.7 Hz, C), 35.8 (d, J = 18.3 Hz, C), 33.7 (s, CH_2), 30.3 (br, CH_3), 29.1 (d, J = 5.0 Hz, CH_3), 26.5 (d, J = 1.6 Hz, CH_2). ^{31}P{^{1}H} NMR (162 MHz; C_6D_6): δ 118.1 (minor isomer), 113.2 (main isomer).

Complex 6. Crystalline **6** was obtained in two different ways. The first method closely followed the procedure reported above for **5** except that benzene was replaced by hexane. Crystals of **6** suitable for X-ray analysis formed in an NMR tube filled with the hexane product solution retrieved from the Parr reactor. The second sample of crystalline **6** was obtained from a benzene/hexane solvent mixture as follows. In an argon glovebox, anhydrous THF (10 mL) was pipetted into a 100 mL round-bottom flask containing **11** (0.6 g, 1.25 mmol) and *t*BuOK (0.18 g, 1.60 mmol), and the mixture was magnetically stirred for 1 h. After solvent removal, the dark-green solid was dried for 1 h under vacuum. This material was extracted with 15 mL of benzene. The dark-green solution was filtered and transferred into the glass liner of a 300 mL Parr autoclave. Further 27 mL of hexane was added, and the reactor was removed from the glovebox, pressurized to 50 bar H_2, and left at room temperature for 4 h without heating or stirring. Next, the autoclave was depressurized, taken back into the glovebox, and opened to reveal a dark red-brown solution. The reactor was closed, repressurized to 50 bar, and left at room temperature for 3 days. When the reactor was opened again in the argon glovebox, there was a dark brown solution and a cluster of large crystals at the bottom. The solution was decanted, and the crystals (∼70 mg) were rinsed with hexane and collected into a vial. The product was characterized by X-ray diffraction and by NMR spectroscopy in C_6D_6 where the crystalline material is very sparingly soluble. The solubility was also poor in CD_2Cl_2 where the product decomposed. Although the principal resonances are well-defined in the ^{1}H NMR spectrum of **6**, there are areas of signal overlap where a detailed interpretation is challenging. The spectrum is also complicated by the resonances of the cocrystallized benzene and hexane. ^{1}H NMR (400 MHz; C_6D_6): δ 8.89 (d, J = 5.0 Hz, 1H), 6.99 (t, J = 7.8 Hz, 1H), 6.93 (dd, J = 7.5, 1.1 Hz, 1H), 6.83 (m, 2H), 6.45 (m, 2H), 5.56 (t, J = 5.2 Hz, 1H), 4.27 (dd, J = 16.9, 6.3 Hz, 1H), 3.77 (m, 2H), 3.68 (d, J = 3.1 Hz, 1H), 3.57 (br, 1H), 3.26 (dd, J = 16.9, 11.0 Hz, 1H), 3.05 (q, J = 11.8 Hz, 1H), 2.54 (m, 2H), 2.22 (m, 1H), 2.00 (m, 1H), 1.66 (m, 7H),

https://dx.doi.org/10.1021/jacs.0c06518
J. Am. Chem. Soc. XXXX, XXX, XXX−XXX

1.48 (m), 1.25 (dd, J = 12.2, 9H), 1.24 (dd, J = 13.1, 9H), 1.17 (d, J = 12.0, 9H), 1.15 (d, J = 12.3, 9H), −10.47 (ddd, J = 23.4, 19.0, 5.0 Hz, 1H), −12.20 (ddt, J = 38.7, 5.9, 5.2 Hz, 1H), −15.72 (dd, J = 30.1, 5.1 Hz, 1H). $^{31}P\{^1H\}$ NMR (162 MHz; C_6D_6): δ 113.6, 98.7.

NMR Data for 7. ^1H NMR (300 MHz; THF-d_8, −30 °C): δ 7.94 (d, J = 5.5 Hz, 1H), 7.83 (d, J = 6.0 Hz, 1H), 7.06 (t, J = 7.6 Hz, 1H), 6.94 (t, J = 7.6 Hz, 1H), 6.80 (d, J = 8.2 Hz, 1H), 6.74 (d, J = 8.2 Hz, 1H), 6.68 (m, 2H), 6.65 (d, J = 6.7 Hz, 1H), 6.58 (d, J = 8.5 Hz, 1H), 6.47 (d, J = 7.1 Hz, 1H), 6.40 (t, J = 6.3 Hz, 1H), 6.01 (m, 2H), 3.21 (dd, J = 11.4, 15.5 Hz, 1H), 3.07 (dd, J = 11.4, 15.6 Hz, 1H), 2.49 (dd, J = 7.9, 15.5 Hz, 1H), 2.37 (dd, J = 6.7, 15.6 Hz, 1H), 1.60 (d, J = 12.0 Hz, CH_3), 1.25 (br, CH_3), 1.07 (br, CH_3), 0.86 (d, J = 11.5 Hz, CH_3), −13.40 (ddd, J = 2.4, 16.0, 23.7 Hz, 1H), −20.05 (ddd, J = 4.3, 12.1, 16.0 Hz, 1H). $^{31}P\{^1H\}$ NMR (300 MHz; THF-d_8): δ 104.8 (s), 122.7 (s).

NMR Data for 9 (Main Species) Formed upon Dissolving 5 in Ethanol-d_6. ^1H NMR (400 MHz; ethanol-d_6): δ 9.01 (m, 1H, Py), 7.84 (td, J = 7.8, 1.6 Hz, 1H, Py), 7.34 (overlapped m, 2H, Py), 3.98 (d, J = 11.6 Hz, 1H, NCH), 3.06 (t, J = 11.6 Hz, 1H, NCH), 2.40−1.63 (m, 8H, CH_2), 1.38 (d, J = 13.2 Hz, 9H, CH_3), 1.35 (d, J = 13.2 Hz, 9H, CH_3), −16.68 (d, J = 26 Hz, 1H). $^{13}C\{^1H\}$ NMR (100 MHz; ethanol-d_6): δ 206.5 (d, J = 15.7 Hz, CO), 164.6, 153.5, 137.7, 124.0, 121.8 (Py), 69.0 (d, J = 2.9 Hz, NCH), 65.1 (m, NCH), 38.0 (d, J = 14.7 Hz, C, t-Bu), 37.6 (d, J = 23.9 Hz, C, t-Bu), 34.4 (d, J = 15.1 Hz, CH_2), 32.3 (d, J = 11.9 Hz, CH_2), 30.4 (d, J = 4.6 Hz, CH_3, t-Bu), 30.3 (d, J = 3.4 Hz, CH_3, t-Bu), 28.2 (s, CH_2), 25.4 (s, CH_2). Resonances of the $Ru(OC_2D_5)$ group were not observed due to exchange with the solvent. $^{31}P\{^1H\}$ NMR (162 MHz; ethanol-d_6): δ 98.5 (s).

NMR Data for 10 Formed on Heating 2 in EtOH for 6 h at 80 °C. ^1H NMR (400 MHz; EtOH): δ 9.00 (m, 1H, Py), 7.84 (td, J = 7.8, 1.6 Hz, 1H, Py), 7.34 (overlapped m, 2H, Py), 3.99 (d, ^3J = 11.2 Hz, 1H, NCH), 3.05 (t, ^3J = 12.2 Hz, 1H, NCH), 2.44−1.63 (m, 8H, CH_2), 1.35 (d, ^3J = 12.8 Hz, 9H, CH_3), 1.31 (d, ^3J = 13.0 Hz, 9H, CH_3), −17.56 (d, ^2J = 26.4 Hz, 1H). $^{13}C\{^1H\}$ NMR (100 MHz; EtOH): δ 205 (d, ^2J = 14.9 Hz, CO), 181.9 (s, OAc), 164.4, 153.7, 137.5, 124.0, 120.9 (Py), 68.1 (d, J = 3.1 Hz, NCH), 64.1 (d, J = 2.6 Hz, NCH), 37.2 (d, J = 23.7 Hz, C, t-Bu), 37.0 (d, J = 15.3 Hz, C, t-Bu), 34.3 (d, J = 15.7 Hz, CH_2), 32.3 (d, J = 12.1 Hz, CH_2), 29.7 (d, J = 3.3 Hz, CH_3, t-Bu), 29.4 (d, J = 4.5 Hz, CH_3, t-Bu), 28.4 (s, CH_2), 24.9 (s, CH_2), 25.4 (s, OAc). $^{31}P\{^1H\}$ NMR (162 MHz; ethanol-d_6): δ 100.1 (s)

Hydrogenation. The hydrogenations of ethyl acetate and methyl hexanoate were performed in a 300 mL stainless-steel Parr reactor. Inside an argon glovebox, the required quantities of the catalysts (9−10 mg) were weighed out on a calibrated analytical balance accurate to 0.1 mg. A balance accurate to 1 mg was used for taking 0.2 mol of the esters (prior to weighing, the ester substrate was allowed to pass through a layer of activated basic alumina). The reactor was loaded with a 0.95 cm × 2.54 cm SCIENCEWARE rare-earth magnet spinbar, the catalyst, and the ester substrate; it was assembled inside the glovebox, then taken outside and pressurized under H_2 to 50 bar. The pressurized reactor was disconnected from the H_2 tank and placed into an oil bath preheated to 100 °C on a hot plate stirrer. This temperature was maintained for 3 h while magnetically stirring at 500 rpm.

Computational Details. All calculated ruthenium species of this paper possess a zero net charge. The DFT calculations were carried out with Gaussian 16, revision c.01,[89] using the M06-L[67,90] and M06-2X functionals.[66] The basis sets used for the initial geometry optimization and frequency calculations on the ruthenium species included def2-QZVP (with def2 ECP) for Ru, and def2-TZVP for all other atoms (together with the W06 density fitting basis set).[91,92] Subsequently, all geometries were reoptimized using the def2-QZVP basis set for all atoms. The polarizable continuum model (asymmetric isotropic IEFPCM) was used in all (except H_2) geometry optimizations and frequency calculations, with the radii and nonelectrostatic terms of Truhlar and co-workers' SMD solvation model (scrf = smd).[93] An example of a typical g16 input file is provided in the Supporting Information. The reported energies of the ruthenium species were obtained by combining the electronic energies of the structures optimized at the M06-L/def2-QZVP level with the thermal corrections from the frequency calculations, plus the standard state correction[94,95] of 1.89 kcal/mol. The standard state correction for ethyl acetate was 3.27 kcal/mol when the ester was both the substrate and the solvent, in Schemes 9−13. All organic molecules (acetaldehyde, ethanol, ethyl acetate, 1-ethoxyethanol) and TS**9** were optimized using the M06-L/def2-QZVP and M06-2X/def2-QZVP methods, followed by frequency calculations at the same level of theory. The nature of the following transition states TS**2**, TS**4**, TS**5**, and TS**11** was confirmed by intrinsic reaction coordinate (IRC) calculations. Dynamics has not been taken into account when modeling the structures with the explicit, hydrogen-bonded ethanol.

■ ASSOCIATED CONTENT

Supporting Information

The Supporting Information is available free of charge at https://pubs.acs.org/doi/10.1021/jacs.0c06518.

Representative NMR spectra, computed energies, and a summary of the crystal data collection and refinement parameters for **5**, **6**, and **7** (PDF)

Crystallographic data for **5**, **6**, and **7** (CIF)

File structures.xyz containing Cartesian coordinates of the metal complexes computed in this study, where this file may be opened as a text file to read the coordinates or opened directly by a molecular modeling program such as Mercury (http://www.ccdc.cam.ac.uk/pages/Home.aspx) for visualization and analysis (XYZ)

■ AUTHOR INFORMATION

Corresponding Authors

Eugene Khaskin − *Okinawa Institute of Science and Technology, Okinawa 904-0495, Japan;* orcid.org/0000-0003-1790-704X; Email: eugene.khaskin@oist.jp

Dmitry G. Gusev − *Department of Chemistry and Biochemistry, Wilfrid Laurier University, Waterloo, ON N2L 3C5, Canada;* orcid.org/0000-0003-3302-356X; Email: dgoussev@wlu.ca

Authors

Louise N. Dawe − *Department of Chemistry and Biochemistry, Wilfrid Laurier University, Waterloo, ON N2L 3C5, Canada;* orcid.org/0000-0003-3630-990X

Morteza Karimzadeh-Younjali − *Department of Chemistry and Biochemistry, Wilfrid Laurier University, Waterloo, ON N2L 3C5, Canada*

Zengjin Dai − *Department of Chemistry and Biochemistry, Wilfrid Laurier University, Waterloo, ON N2L 3C5, Canada*

Complete contact information is available at: https://pubs.acs.org/10.1021/jacs.0c06518

Funding

Natural Sciences and Engineering Research Council (NSERC) of Canada, Discovery grant program, and Compute Canada.

Notes

The authors declare no competing financial interest.

■ ACKNOWLEDGMENTS

D.G.G. is thankful to the NSERC of Canada—Discovery grant program, CFI LOF program, Compute Canada, and Wilfrid Laurier University for support. Dr. Paul D. Boyle, the University of Western Ontario, is acknowledged for assistance with the X-ray data collection.

https://dx.doi.org/10.1021/jacs.0c06518
J. Am. Chem. Soc. XXXX, XXX, XXX−XXX

REFERENCES

(1) Zhang, J.; Leitus, G.; Ben-David, Y.; Milstein, D. Facile Conversion of Alcohols into Esters and Dihydrogen Catalyzed by New Ruthenium Complexes. *J. Am. Chem. Soc.* **2005**, *127*, 10840−10841.

(2) Zhang, J.; Leitus, G.; Ben-David, Y.; Milstein, D. Efficient Homogeneous Catalytic Hydrogenation of Esters to Alcohols. *Angew. Chem., Int. Ed.* **2006**, *45*, 1113−1115.

(3) Balaraman, E.; Gnanaprakasam, B.; Shimon, L. J. W.; Milstein, D. Direct Hydrogenation of Amides to Alcohols and Amines under Mild Conditions. *J. Am. Chem. Soc.* **2010**, *132*, 16756−16758.

(4) Balaraman, E.; Ben-David, Y.; Milstein, D. Unprecedented Catalytic Hydrogenation of Urea Derivatives to Amines and Methanol. *Angew. Chem., Int. Ed.* **2011**, *50*, 11702−11705.

(5) Balaraman, E.; Gunanathan, C.; Zhang, J.; Shimon, L. J. W.; Milstein, D. Efficient Hydrogenation of Organic Carbonates, Carbamates and Formates Indicates Alternative Routes to Methanol Based on CO_2 and CO. *Nat. Chem.* **2011**, *3*, 609−614.

(6) Milstein, D. Discovery of Environmentally Benign Catalytic Reactions of Alcohols Catalyzed by Pyridine-Based Pincer Ru Complexes, Based on Metal−Ligand Cooperation. *Top. Catal.* **2010**, *53*, 915−923.

(7) Gunanathan, C.; Milstein, D. Bond Activation by Metal−Ligand Cooperation: Design of "Green" Catalytic Reactions Based on Aromatization−Dearomatization of Pincer Complexes. *Top. Organomet. Chem.* **2011**, *37*, 55−84.

(8) Gunanathan, C.; Milstein, D. Metal-Ligand Cooperation by Aromatization-Dearomatization: A New Paradigm in Bond Activation and "Green" Catalysis. *Acc. Chem. Res.* **2011**, *44*, 588−602.

(9) Gunanathan, C.; Milstein, D. Bond Activation and Catalysis by Ruthenium Pincer Complexes. *Chem. Rev.* **2014**, *114*, 12024−12087.

(10) Gunanathan, C.; Milstein, D. Catalysis by Pincer Complexes: Synthesis of Esters, Amides, and Peptides. In *Pincer and Pincer-Type Complexes: Applications in Organic Synthesis and Catalysis*; Szabó, K. J., Wendt, O. F., Eds.; Wiley-VCH Verlag GmbH & Co. KGaA, 2014.

(11) Khusnutdinova, J. R.; Milstein, D. Metal−Ligand Cooperation. *Angew. Chem., Int. Ed.* **2015**, *54*, 12236−12273.

(12) Milstein, D. Metal−Ligand Cooperation by Aromatization-Dearomatization as a Tool in Single Bond Activation. *Philos. Trans. R. Soc., A* **2015**, *373*, 20140189.

(13) Grützmacher, H. Cooperating Ligands in Catalysis. *Angew. Chem., Int. Ed.* **2008**, *47*, 1814−1818.

(14) Gelman, D.; Musa, S. Coordination Versatility of sp^3-Hybridized Pincer Ligands toward Ligand−Metal Cooperative Catalysis. *ACS Catal.* **2012**, *2*, 2456−2466.

(15) Dub, P. A.; Ikariya, T. Catalytic Reductive Transformations of Carboxylic and Carbonic Acid Derivatives Using Molecular Hydrogen. *ACS Catal.* **2012**, *2*, 1718−1741.

(16) Eisenstein, O.; Crabtree, R. H. Outer Sphere Hydrogenation Catalysis. *New J. Chem.* **2013**, *37*, 21−27.

(17) Werkmeister, S.; Junge, K.; Beller, M. Catalytic Hydrogenation of Carboxylic Acid Esters, Amides, and Nitriles with Homogeneous Catalysts. *Org. Process Res. Dev.* **2014**, *18*, 289−302.

(18) Trincado, M.; Banerjee, D.; Grützmacher, H. Molecular Catalysts for Hydrogen Production from Alcohols. *Energy Environ. Sci.* **2014**, *7*, 2464−2503.

(19) Werkmeister, S.; Neumann, J.; Junge, K.; Beller, M. Pincer-Type Complexes for Catalytic (De)Hydrogenation and Transfer (De)-Hydrogenation Reactions: Recent Progress. *Chem. - Eur. J.* **2015**, *21*, 12226−12250.

(20) Younus, H. A.; Su, W.; Ahmad, N.; Chen, S.; Verpoort, F. Ruthenium Pincer Complexes: Synthesis and Catalytic Applications. *Adv. Synth. Catal.* **2015**, *357*, 283−330.

(21) Crabtree, R. H. Homogeneous Transition Metal Catalysis of Acceptorless Dehydrogenative Alcohol Oxidation: Applications in Hydrogen Storage and to Heterocycle Synthesis. *Chem. Rev.* **2017**, *117*, 9228−9246.

(22) Dub, P. A.; Gordon, J. C. Metal-Ligand Bifunctional Catalysis: The "Accepted" Mechanism, the Issue of Concertedness, and the Function of the Ligand in Catalytic Cycles Involving Hydrogen Atoms. *ACS Catal.* **2017**, *7*, 6635−6655.

(23) Hale, L. V. A.; Szymczak, N. K. Hydrogen Transfer Catalysis beyond the Primary Coordination Sphere. *ACS Catal.* **2018**, *8*, 6446−6461.

(24) Li, J.; Shiota, Y.; Yoshizawa, K. Metal−Ligand Cooperation in H_2 Production and H_2O Decomposition on a Ru(II) PNN Complex: The Role of Ligand Dearomatization−Aromatization. *J. Am. Chem. Soc.* **2009**, *131*, 13584−13585.

(25) Gusev, D. G. Revised Mechanisms of the Catalytic Alcohol Dehydrogenation and Ester Reduction with the Milstein PNN Complex of Ruthenium. *Organometallics* **2020**, *39*, 258−270.

(26) Huff, C. A.; Sanford, M. S. Cascade Catalysis for the Homogeneous Hydrogenation of CO_2 to Methanol. *J. Am. Chem. Soc.* **2011**, *133*, 18122−18125.

(27) Gnanaprakasam, B.; Balaraman, E.; Gunanathan, C.; Milstein, D. Synthesis of Polyamides from Diols and Diamines with Liberation of H_2. *J. Polym. Sci., Part A: Polym. Chem.* **2012**, *50*, 1755−1765.

(28) Srimani, D.; Balaraman, E.; Gnanaprakasam, B.; Ben-David, Y.; Milstein, D. Ruthenium Pincer-Catalyzed Cross-Dehydrogenative Coupling of Primary Alcohols with Secondary Alcohols under Neutral Conditions. *Adv. Synth. Catal.* **2012**, *354*, 2403−2406.

(29) Balaraman, E.; Fogler, E.; Milstein, D. Efficient Hydrogenation of Biomass-Derived Cyclic Di-Esters to 1,2-Diols. *Chem. Commun.* **2012**, *48*, 1111−1113.

(30) Srimani, D.; Feller, M.; Ben-David, Y.; Milstein, D. Catalytic Coupling of Nitriles with Amines to Selectively Form Imines Under Mild Hydrogen Pressure. *Chem. Commun.* **2012**, *48*, 11853−11855.

(31) Khaskin, E.; Milstein, D. Simple and Efficient Catalytic Reaction for the Selective Deuteration of Alcohols. *ACS Catal.* **2013**, *3*, 448−452.

(32) Srimani, D.; Balaraman, E.; Hu, P.; Ben-David, Y.; Milstein, D. Formation of Tertiary Amides and Dihydrogen by Dehydrogenative Coupling of Primary Alcohols with Secondary Amines Catalyzed by Ruthenium Bipyridine-Based Pincer Complexes. *Adv. Synth. Catal.* **2013**, *355*, 2525−2530.

(33) Srimani, D.; Ben-David, Y.; Milstein, D. Direct Synthesis of Pyrroles by Dehydrogenative Coupling of β-Aminoalcohols with Secondary Alcohols Catalyzed by Ruthenium Pincer Complexes. *Angew. Chem., Int. Ed.* **2013**, *52*, 4012−4015.

(34) Srimani, D.; Ben-David, Y.; Milstein, D. Direct Synthesis of Pyridines and Quinolines by Coupling of γ-Amino-alcohols with Secondary Alcohols Liberating H_2 Catalyzed by Ruthenium Pincer Complexes. *Chem. Commun.* **2013**, *49*, 6632−6634.

(35) Balaraman, E.; Khaskin, E.; Leitus, G.; Milstein, D. Catalytic Transformation of Alcohols to Carboxylic Acid Salts and H_2 Using Water as the Oxygen Atom Source. *Nat. Chem.* **2013**, *5*, 122−125.

(36) Hu, P.; Diskin-Posner, Y.; Ben-David, Y.; Milstein, D. Reusable Homogeneous Catalytic System for Hydrogen Production from Methanol and Water. *ACS Catal.* **2014**, *4*, 2649−2652.

(37) Srimani, D.; Leitus, G.; Ben-David, Y.; Milstein, D. Direct Catalytic Olefination of Alcohols with Sulfones. *Angew. Chem., Int. Ed.* **2014**, *53*, 11092−11095.

(38) Krall, E. M.; Klein, T. W.; Andersen, R. J.; Nett, A. J.; Glasgow, R. W.; Reader, D. S.; Dauphinais, B. C.; Mc Ilrath, S. P.; Fischer, A. A.; Carney, M. J.; Hudson, D. J.; Robertson, N. J. Controlled Hydrogenative Depolymerization of Polyesters and Polycarbonates Catalyzed by Ruthenium(II) PNN Pincer Complexes. *Chem. Commun.* **2014**, *50*, 4884−4887.

(39) Balaraman, E.; Srimani, D.; Diskin-Posner, Y.; Milstein, D. Direct Synthesis of Secondary Amines From Alcohols and Ammonia Catalyzed by a Ruthenium Pincer Complex. *Catal. Lett.* **2015**, *145*, 139−144.

(40) Khusnutdinova, J. R.; Garg, J. A.; Milstein, D. Combining Low-Pressure CO_2 Capture and Hydrogenation to Form Methanol. *ACS Catal.* **2015**, *5*, 2416−2422.

(41) Khaskin, E.; Milstein, D. Catalytic, Oxidant-Free, Direct Olefination of Alcohols using Wittig Reagents. *Chem. Commun.* **2015**, *51*, 9002−9005.

https://dx.doi.org/10.1021/jacs.0c06518
J. Am. Chem. Soc. XXXX, XXX, XXX−XXX

(42) Hu, P.; Ben-David, Y.; Milstein, D. Rechargeable Hydrogen Storage System Based on the Dehydrogenative Coupling of Ethylenediamine with Ethanol. *Angew. Chem., Int. Ed.* **2016**, *55*, 1061−1064.
(43) Zeng, R.; Feller, M.; Diskin-Posner, Y.; Shimon, L. J. W.; Ben-David, Y.; Milstein, D. CO Oxidation by N_2O Homogeneously Catalyzed by Ruthenium Hydride Pincer Complexes Indicating a New Mechanism. *J. Am. Chem. Soc.* **2018**, *140*, 7061−7064.
(44) Cantillo, D. Mechanistic Insights on the Ruthenium-Catalyzed Hydrogenation of Amides − C−N vs. C−O Cleavage. *Eur. J. Inorg. Chem.* **2011**, *2011*, 3008−3013.
(45) Li, H.; Hall, M. B. Mechanism of the Formation of Carboxylate from Alcohols and Water Catalyzed by a Bipyridine-Based Ruthenium Complex: A Computational Study. *J. Am. Chem. Soc.* **2014**, *136*, 383−395.
(46) Qu, S.; Dang, Y.; Song, C.; Wen, M.; Huang, K.-W.; Wang, Z.-X. Catalytic Mechanisms of Direct Pyrrole Synthesis via Dehydrogenative Coupling Mediated by PNP-Ir or PNN-Ru Pincer Complexes: Crucial Role of Proton-Transfer Shuttles in the PNP-Ir System. *J. Am. Chem. Soc.* **2014**, *136*, 4974−4991.
(47) Zhang, H. A. DFT study on direct hydrogenation of amide catalyzed by a PNN Ru(II) pincer complex. *Comput. Theor. Chem.* **2015**, *1066*, 1−6.
(48) Hasanayn, F.; Al-Assi, L. M.; Moussawi, R. N.; Omar, B. S. Mechanism of Alcohol−Water Dehydrogenative Coupling into Carboxylic Acid Using Milstein's Catalyst: A Detailed Investigation of the Outer-Sphere PES in the Reaction of Aldehydes with an Octahedral Ruthenium Hydroxide. *Inorg. Chem.* **2016**, *55*, 7886−7902.
(49) Gonçalves, T. P.; Huang, K.-W. Metal−Ligand Cooperative Reactivity in the (Pseudo)-Dearomatized PNx(P) Systems: The Influence of the Zwitterionic Form in Dearomatized Pincer Complexes. *J. Am. Chem. Soc.* **2017**, *139*, 13442−13449.
(50) Spasyuk, D.; Smith, S.; Gusev, D. G. From Esters to Alcohols and Back with Ruthenium and Osmium Catalysts. *Angew. Chem., Int. Ed.* **2012**, *51*, 2772−2775.
(51) Spasyuk, D.; Gusev, D. G. Acceptorless Dehydrogenative Coupling of Ethanol and Hydrogenation of Esters and Imines. *Organometallics* **2012**, *31*, 5239−5242.
(52) Spasyuk, D.; Vicent, C.; Gusev, D. G. Chemoselective Hydrogenation of Carbonyl Compounds and Acceptorless Dehydrogenative Coupling of Alcohols. *J. Am. Chem. Soc.* **2015**, *137*, 3743−3746.
(53) Gusev, D. G. Dehydrogenative Coupling of Ethanol and Ester Hydrogenation Catalyzed by Pincer-type YNP Complexes. *ACS Catal.* **2016**, *6*, 6967−6981.
(54) Wang, Z.; Li, Y.; Liu, Q.; Solan, G. A.; Ma, Y.; Sun, W. Direct Hydrogenation of a Broad Range of Amides under Base-free Conditions using an Efficient and Selective Ruthenium(II) Pincer Catalyst. *ChemCatChem* **2017**, *9*, 4275−4281.
(55) Wang, Z.; Chen, X.; Liu, B.; Liu, Q.; Solan, G. A.; Yang, X.; Sun, W. Cooperative Interplay Between a Flexible PNN-Ru(II) Complex and a $NaBH_4$ Additive in the Efficient Catalytic Hydrogenation of Esters. *Catal. Sci. Technol.* **2017**, *7*, 1297−1304.
(56) He, T.; Buttner, J. C.; Reynolds, E. F.; Pham, J.; Malek, J. C.; Keith, J. M.; Chianese, A. R. Dehydroalkylative Activation of CNN- and PNN-Pincer Ruthenium Catalysts for Ester Hydrogenation. *J. Am. Chem. Soc.* **2019**, *141*, 17404−17413.
(57) Nguyen, D. H.; Trivelli, X.; Capet, F.; Swesi, Y.; Favre-Réguillon, A.; Vanoye, L.; Dumeignil, F.; Gauvin, R. M. Deeper Mechanistic Insight into Ru Pincer-Mediated Acceptorless Dehydrogenative Coupling of Alcohols: Exchanges, Intermediates, and Deactivation Species. *ACS Catal.* **2018**, *8*, 4719−4734.
(58) Zweifel, T.; Naubron, J.-V.; Büttner, T.; Ott, T.; Grützmacher, H. Ethanol as Hydrogen Donor: Highly Efficient Transfer Hydrogenations with Rhodium(I) Amides. *Angew. Chem., Int. Ed.* **2008**, *47*, 3245−3249.
(59) Hasanayn, F.; Baroudi, A. Direct H/OR and OR/OR′ Metathesis Pathways in Ester Hydrogenation and Transesterification by Milstein's Catalyst. *Organometallics* **2013**, *32*, 2493−2496.
(60) Dub, P. A.; Henson, N. J.; Martin, R. L.; Gordon, J. C. Unravelling the Mechanism of the Asymmetric Hydrogenation of Acetophenone by [RuX_2(diphosphine)(1,2-diamine)] Catalysts. *J. Am. Chem. Soc.* **2014**, *136*, 3505−3521.
(61) Dub, P. A.; Gordon, J. C. The Mechanism of Enantioselective Ketone Reduction with Noyori and Noyori-Ikariya Bifunctional Catalysts. *Dalton Trans.* **2016**, *45*, 6756−6781.
(62) Dub, P. A.; Scott, B. L.; Gordon, J. C. Why Does Alkylation of the N-H Functionality within M/NH Bifunctional Noyori-Type Catalysts Lead to Turnover? *J. Am. Chem. Soc.* **2017**, *139*, 1245−1260.
(63) Dub, P. A.; Gordon, J. C. The Role of the Metal-Bound N−H Functionality in Noyori-type Molecular Catalysts. *Nat. Rev. Chem.* **2018**, *2*, 396−408.
(64) Dub, P. A.; Batrice, R. J.; Gordon, J. C.; Scott, B. L.; Minko, Y.; Schmidt, J. G.; Williams, R. F. Engineering Catalysts for Selective Ester Hydrogenation. *Org. Process Res. Dev.* **2020**, *24* (3), 415−442.
(65) Morris, S. A.; Gusev, D. G. Rethinking the Claisen−Tishchenko Reaction. *Angew. Chem., Int. Ed.* **2017**, *56*, 6228−6231.
(66) Zhao, Y.; Truhlar, D. G. The M06 Suite of Density Functionals for Main Group Thermochemistry, Thermochemical Kinetics, Noncovalent Interactions, Excited States, and Transition Elements: Two New Functionals and Systematic Testing of Four M06-class Functionals and 12 Other Functionals. *Theor. Chem. Acc.* **2008**, *120*, 215−241.
(67) Gusev, D. G. Assessing the Accuracy of M06-L Thermochemistry. *Organometallics* **2013**, *32*, 4239−4243.
(68) Ikariya, T. Bifunctional Transition Metal-Based Molecular Catalysts for Asymmetric Syntheses. *Top. Organomet. Chem.* **2011**, *37*, 31−53.
(69) *Hydrogen and Deuterium*; Young, C. L., Ed.; IUPAC Solubility Data Series, Vol. 5/6; Pergamon Press: New York, 1981; p 231.
(70) Ribeiro, R. F.; Marenich, A. V.; Cramer, C. J.; Truhlar, D. G. Use of Solution-Phase Vibrational Frequencies in Continuum Models for the Free Energy of Solvation. *J. Phys. Chem. B* **2011**, *115*, 14556−14562.
(71) Langer, R.; Fuchs, I.; Vogt, M.; Balaraman, E.; Diskin-Posner, Y.; Shimon, L. J. W.; Ben-David, Y.; Milstein, D. Stepwise Metal−Ligand Cooperation by a Reversible Aromatization/Deconjugation Sequence in Ruthenium Complexes with a Tetradentate Phenanthroline-Based Ligand. *Chem. - Eur. J.* **2013**, *19*, 3407−3414.
(72) Miura, T.; Held, I. E.; Oishi, S.; Naruto, M.; Saito, S. Catalytic Hydrogenation of Unactivated Amides Enabled by Hydrogenation of Catalyst Precursor. *Tetrahedron Lett.* **2013**, *54*, 2674−2678.
(73) Miura, T.; Naruto, M.; Toda, K.; Shimomura, T.; Saito, S. Multifaceted Catalytic Hydrogenation of Amides via Diverse Activation of a Sterically Confined Bipyridine−Ruthenium Framework. *Sci. Rep.* **2017**, *7*, 1586.
(74) Nimura, S.; Yoshioka, S.; Naruto, M.; Saito, S. Reaction of H_2 with Mitochondria-Relevant Metabolites using a Multifunctional Molecular Catalyst. *ChemRxiv* **2020**, DOI: 10.26434/chemrxiv.11994471.v1.
(75) Das, U. K.; Ben-David, Y.; Diskin-Posner, Y.; Milstein, D. N-Substituted Hydrazones by Manganese-Catalyzed Coupling of Alcohols with Hydrazine: Borrowing Hydrogen and Acceptorless Dehydrogenation in One System. *Angew. Chem., Int. Ed.* **2018**, *57*, 2179−2182.
(76) Das, U. K.; Ben-David, Y.; Leitus, G.; Diskin-Posner, Y.; Milstein, D. Dehydrogenative Cross-Coupling of Primary Alcohols To Form Cross-Esters Catalyzed by a Manganese Pincer Complex. *ACS Catal.* **2019**, *9*, 479−484.
(77) Das, U. K.; Kumar, A.; Ben-David, Y.; Iron, M. A.; Milstein, D. Manganese Catalyzed Hydrogenation of Carbamates and Urea Derivatives. *J. Am. Chem. Soc.* **2019**, *141*, 12962−12966.
(78) Das, U. K.; Janes, T.; Kumar, A.; Milstein, D. Manganese Catalyzed Selective Hydrogenation of Cyclic Imides to Diols and Amines. *Green Chem.* **2020**, *22*, 3079−3082.
(79) Zhang, L.; Peng, D.; Leng, X.; Huang, Z. Iron-Catalyzed, Atom-Economical, Chemo- and Regioselective Alkene Hydroboration with Pinacolborane. *Angew. Chem., Int. Ed.* **2013**, *52*, 3676−3680.
(80) Zell, T.; Langer, R.; Iron, M. A.; Konstantinovski, L.; Shimon, L. J. W.; Diskin-Posner, Y.; Leitus, G.; Balaraman, E.; Ben-David, Y.; Milstein, D. Synthesis, Structures, and Dearomatization by Deproto-

https://dx.doi.org/10.1021/jacs.0c06518
J. Am. Chem. Soc. XXXX, XXX, XXX−XXX

nation of Iron Complexes Featuring Bipyridine-based PNN Pincer Ligands. *Inorg. Chem.* **2013**, *52*, 9636−9649.
(81) Jia, X.; Zhang, L.; Qin, C.; Leng, X.; Huang, Z. Iridium Complexes of New NCP Pincer Ligands: Catalytic Alkane Dehydrogenation and Alkene Isomerization. *Chem. Commun.* **2014**, *50*, 11056−11059.
(82) Zell, T.; Milko, P.; Fillman, K. L.; Diskin-Posner, Y.; Bendikov, T.; Iron, M. A.; Leitus, G.; Ben-David, Y.; Neidig, M. L.; Milstein, D. Iron Dicarbonyl Complexes Featuring Bipyridine-Based PNN Pincer Ligands with Short Interpyridine CC Bond Lengths: Innocent or Non-Innocent Ligand? *Chem. - Eur. J.* **2014**, *20*, 4403−4413.
(83) Cummins, A. W. M.; Li, S.; Willcox, D. R.; Muilu, T.; Docherty, J. H.; Thomas, S. P. Synthesis of DBpin Using Earth-abundant Metal Catalysis. *Tetrahedron* **2020**, *76*, 131084.
(84) Zhang, L.; Zuo, Z.; Leng, X.; Huang, Z. A Cobalt-Catalyzed Alkene Hydroboration with Pinacolborane. *Angew. Chem., Int. Ed.* **2014**, *53*, 2696−2700.
(85) Schaefer, B. A.; Margulieux, G. W.; Small, B. L.; Chirik, P. J. Evaluation of Cobalt Complexes Bearing Tridentate Pincer Ligands for Catalytic C−H Borylation. *Organometallics* **2015**, *34*, 1307−1320.
(86) Zhang, L.; Huang, Z. Synthesis of 1,1,1-Tris(boronates) from Vinylarenes by Co-Catalyzed Dehydrogenative Borylations−Hydroboration. *J. Am. Chem. Soc.* **2015**, *137*, 15600−15603.
(87) Wen, H.; Zhang, L.; Zhu, S.; Liu, G.; Huang, Z. Stereoselective Synthesis of Trisubstituted Alkenes via Cobalt-Catalyzed Double Dehydrogenative Borylations of 1-Alkenes. *ACS Catal.* **2017**, *7*, 6419−6425.
(88) Qiao, L.; Zhang, L.; Liu, G.; Huang, Z. A Highly Efficient Cobalt-catalyzed Deuterogenolysis of Diboron: Synthesis of Deuterated Pinacolborane and Vinylboronates. *Tetrahedron* **2019**, *75*, 4138−4142.
(89) Frisch, M. J.; Trucks, G. W.; Schlegel, H. B.; Scuseria, G. E.; Robb, M. A.; Cheeseman, J. R.; Scalmani, G.; Barone, V.; Petersson, G. A.; Nakatsuji, H.; Li, X.; Caricato, M.; Marenich, A. V.; Bloino, J.; Janesko, B. G.; Gomperts, R.; Mennucci, B.; Hratchian, H. P.; Ortiz, J. V.; Izmaylov, A. F.; Sonnenberg, J. L.; Williams-Young, D.; Ding, F.; Lipparini, F.; Egidi, F.; Goings, J.; Peng, B.; Petrone, A.; Henderson, T.; Ranasinghe, D.; Zakrzewski, V. G.; Gao, J.; Rega, N.; Zheng, G.; Liang, W.; Hada, M.; Ehara, M.; Toyota, K.; Fukuda, R.; Hasegawa, J.; Ishida, M.; Nakajima, T.; Honda, Y.; Kitao, O.; Nakai, H.; Vreven, T.; Throssell, K.; Montgomery, J. A., Jr.; Peralta, J. E.; Ogliaro, F.; Bearpark, M. J.; Heyd, J. J.; Brothers, E. N.; Kudin, K. N.; Staroverov, V. N.; Keith, T. A.; Kobayashi, R.; Normand, J.; Raghavachari, K.; Rendell, A. P.; Burant, J. C.; Iyengar, S. S.; Tomasi, J.; Cossi, M.; Millam, J. M.; Klene, M.; Adamo, C.; Cammi, R.; Ochterski, J. W.; Martin, R. L.; Morokuma, K.; Farkas, O.; Foresman, J. B.; Fox, D. J. *Gaussian 16*, revision A.03; Gaussian, Inc.: Wallingford, CT, 2016.
(90) Zhao, Y.; Truhlar, D. G. A New Local Density Functional for Main-Group Thermochemistry, Transition Metal Bonding, Thermochemical Kinetics, and Noncovalent Interactions. *J. Chem. Phys.* **2006**, *125*, 194101−194118.
(91) Weigend, F.; Ahlrichs, R. Balanced Basis Sets of Split Valence, Triple Zeta Valence and Quadruple Zeta Valence Quality for H to Rn: Design and Assessment of Accuracy. *Phys. Chem. Chem. Phys.* **2005**, *7*, 3297−3305.
(92) Weigend, F. Accurate Coulomb-Fitting Basis Sets for H to Rn. *Phys. Chem. Chem. Phys.* **2006**, *8*, 1057−1065.
(93) Marenich, A. V.; Cramer, C. J.; Truhlar, D. G. Universal Solvation Model Based on Solute Electron Density and on a Continuum Model of the Solvent Defined by the Bulk Dielectric Constant and Atomic Surface Tensions. *J. Phys. Chem. B* **2009**, *113*, 6378−6396.
(94) Hopmann, K. H. How Accurate is DFT for Iridium-Mediated Chemistry? *Organometallics* **2016**, *35*, 3795−3807.
(95) Harvey, J. N.; Himo, F.; Maseras, F.; Perrin, L. Scope and Challenge of Computational Methods for Studying Mechanism and Reactivity in Homogeneous Catalysis. *ACS Catal.* **2019**, *9*, 6803−6813.

https://dx.doi.org/10.1021/jacs.0c06518
J. Am. Chem. Soc. XXXX, XXX, XXX−XXX